

Interaction Notes

Note 564

February 2001

**Coulomb Gauge Green's Functions
For the Electromagnetic Field**

Robert Nevels
Krzysztof Michalski

Electromagnetics and Microwave Laboratory
Department of Electrical Engineering
Texas A&M University

Abstract

The mixed potential electric field integral equation (MPIE) method is a widely used numerical method in wave scattering analysis. The MPIE and all other classical Maxwell equation scattering methods involving the scalar and vector potentials are based on the Lorentz gauge. In this report we analyze a series of waveguiding and scattering problems formulated by enforcing the Coulomb gauge. Coulomb gauge Green's functions are derived for a rectangular waveguide, free space, a cylinder and a wedge. With the MPIE method the currents on a scatterer are shown to be gauge independent. Comparisons are therefore made between the computation times necessary for calculating the current on a straight thin wire and on arbitrary scatters in the presence of a circular conducting cylinder and conducting wedge. Conclusions are drawn concerning the utility of the Coulomb gauge as compared to the Lorentz and other gauges.

Chapter 1

Introduction

Computers have allowed researchers to solve for the electromagnetic fields radiated and scattered from structures with greater physical detail than could be accounted for by purely analytical means. However, the variety of analytical formulations developed under various geometrical constraints as well as computer storage and run time limitations, have led to a proliferation of numerical solution methods. No single numerical method has been found that can be efficiently applied in all situations, so while certain techniques are widely used, research continues on strategies to improve analytical/numerical formulations which will shorten computation time and extend the physical sophistication of the scattering body.

One numerical method that has gained general acceptance is the integral equation approach, which models conducting or dielectric bodies by surface patches and by volumetric cubes or tetrahedrons. Integral equations models are designed to compute currents from which impedances and near and far fields can be calculated. The most widely used integral equation numerical technique, that is especially useful in near field scattering analysis but comparable to other methods when the far field or radar cross section is to be calculated, is the mixed potential electric field integral equation (MPIE) method described for example in Rao *et.al.* [1]. The MPIE is formulated by expressing the electric and magnetic fields in terms of the electric vector potential (\underline{A}) and scalar potential (ϕ) which are composed of integral and differential operators, the current, and the free space Green's function. Boundary conditions are enforced resulting in an integral equation in terms of an unknown volume current or a surface current, located on the boundary between dielectric regions or on conductor surfaces, that is solved for by the method of moments [1].

The disadvantages of the MPIE method are that the scalar potential operator contains two derivatives and both the scalar and vector potentials have a singular kernel. These are overcome by careful selection of the basis functions that represent the current and charge and the testing functions that produce a linear set of solvable equations and standard numerical methods for singularity removal. The advantages of the MPIE method are that it can be applied to both open and closed bodies and the basis function subdomain dimensions can be adjusted to give more detail in regions where the current changes rapidly with spacial position.

In this report we take advantage of the fact that the MPIE is expressed in terms of potentials, that the potentials are determined by a gauge condition and that the fields are gauge invariant [2]. It is the intention of this investigation to show that integral equation scattering formulations based on gauges other than the Lorentz gauge can improve numerical computation speed and extend the range of applicability of contemporary integral equation scattering models.

In classical electromagnetic field analysis, when the fields are expressed in terms of potentials, the Lorentz gauge historically has been the gauge of choice. An exception to this rule is sometimes made for a small class of problems where the divergence of both the magnetic vector potential \underline{A} and the current density \underline{J} are zero [3]. In that case it is convenient to use what is commonly referred to as the radiation gauge [2]. The label “radiation gauge” is relevant because the conditions described above respectively include and infer the constraints $\underline{\nabla} \cdot \underline{A} = 0$ and $\Phi = 0$ that are associated with a far radiated field.

During the initial stage of this research it was found that there were no classical Maxwell equation scattering models based on the Coulomb gauge ($\underline{\nabla} \cdot \underline{A} = 0, \Phi \neq 0$), except for one incorrect attempt described in a text by Smythe [4]. Because the Coulomb gauge offered an alternative to the Lorentz gauge and because it was as yet, an unsolved problem in scattering analysis, it was decided by the authors that a thorough investigation of the Coulomb gauge would provide the necessary “stepping stone” for other gauge formulations. Consequently the remainder of this report will detail comparisons between the Coulomb and the Lorentz gauge formulations for various scattering configurations and subject to a variety of boundary conditions.

A change in gauge essentially means that the vector and scalar potentials will have

Green's functions other than the familiar Lorentz gauge Green's functions. Comparison between the Lorentz gauge and other gauges can best be displayed by incorporating the effects of some object such as a cylinder or wedge in the Green's function, thereby leaving the current distribution on some nearby arbitrary surface as the only unknown. This approach is sometimes referred to as the hybrid MM/Green's function method [5]. An important consequence of the hybrid MM/Green's function method presented here is that the Green's functions are in their most general (dyadic) form.

In Chapter 2 magnetic vector and scalar potential Green's functions are derived subject to the Coulomb gauge for a general directed source in free space. It is shown that the Coulomb gauge vector potential Green's function can be extracted from the well known free space Lorentz gauge vector potential Green's function by taking advantage of a set of dyadic identities. This method avoids the difficulties associated with deriving dyadic Green's functions from first principles as is done in later chapters.

In order to confirm the correctness of Coulomb gauge potential expressions, MPIE's are derived subject to both Lorentz and Coulomb gauges for a finite length cylinder scatterer. The MPIE's are solved for the cylinder surface current by the method of moments. Because the current is unique (i.e. independent of gauge) it is used in this report as a basis for comparing the Coulomb and Lorentz gauge formulations in Chapters 2, 4 and 5.

The Coulomb gauge method for solving source-excited boundary value problems in closed (waveguide) regions is presented in Chapter 3. Here the vector eigenfunction method [6,7] is used to obtain the dyadic Green's functions. This method was found to be ideally suited for deriving Coulomb gauge Green's functions owing to the particular vector nature (solenoidal) of the Coulomb vector potential.

In Chapter 4 and 5 two two-dimensional open region scattering problems are presented: plane wave scattering from an arbitrary shaped conducting scatterer in the presence of, respectively, a conducting cylinder and a conducting wedge. In these two cases the Lorentz scalar potential is expressed as an infinite series whereas the Coulomb scalar potential is closed form. A closed form scalar potential is seen as one of the primary advantages of the Coulomb gauge over the Lorentz gauge in mixed potential formulations.

Throughout this report numerical simulations of various scattering and waveguidance problems are carried out by incorporating the Coulomb gauge vector potential Green's functions in mixed potential integral equations (MPIE's). The subsequent numerical solutions are verified by comparison with the electric and magnetic current obtained with MPIE's incorporating Lorentz gauge Green's functions. In Chapter 6 it is shown by analytical means that both the field and the conduction current are unique in the sense that they do not depend on gauge. This mathematical verification is carried out in the time, frequency and spectral domains. Uniqueness of the current is a powerful tool since one only need interchange a Coulomb gauge Greens function with its Lorentz gauge counterpart in a MPIE code. The computed current is much more sensitive to inaccuracies in analytical formulation than is the field.

In Chapter 7 we investigate the efficacy of incorporating Coulomb gauge Green's functions in time-domain integral equations. We present some of the obstacles that must be overcome in order to carry out volume and surface current calculations. It is shown that a 3-D integration and solution of a matrix equation at each time step are necessary with the Coulomb gauge, while the Lorentz gauge requires only a 2-D integration and no matrix equation.

Chapter 8 contains our conclusions concerning in particular the Coulomb gauge as compared to the Lorentz gauge and in general the possibility of using other gauges in Maxwell equation scattering formulations. Also in this chapter are our recommendations for future research on alternative gauges.

Chapter 2

Analysis of a Wire Scatterer

In this chapter the magnetic vector and scalar potential Green's functions are derived subject to the Coulomb gauge for a general directed source in free space. Some of the unique features of the Coulomb gauge are discussed followed by a presentation of the MPIE's for a thin, straight, finite-length cylinder scatterer formulated subject to the Lorentz and Coulomb gauges. The chapter concludes with a comparison of Lorentz and Coulomb gauge current distribution and computation time results.

2.1 Fields in Terms of Potentials

The time harmonic electric and magnetic fields are related to the magnetic vector potential \underline{A} and scalar potential Φ according to

$$\underline{E} = -j\omega\underline{A} - \nabla\Phi \quad (2.1)$$

$$\underline{H} = \frac{1}{\mu} \nabla \times \underline{A} \quad (2.2)$$

with the time convention $\exp(j\omega t)$ suppressed. In terms of the cylinder surface current density \underline{J} and the dyadic vector and scalar Green's functions, \underline{G} and G_Φ respectively, the magnetic vector and scalar potentials are [8]:

$$\underline{A}(\underline{r}) = \mu \int_{v'} \underline{G}(\underline{r}|\underline{r}') \cdot \underline{J}(\underline{r}') dv' \quad (2.3)$$

$$\Phi(\underline{r}) = \frac{-1}{j\omega\epsilon} \int_{v'} G_\Phi(\underline{r}|\underline{r}') \nabla' \cdot \underline{J}(\underline{r}') dv' \quad (2.4)$$

2.2 Lorentz Gauge Green's Functions in Free Space

The mathematical form taken on by the Green's functions depends upon the gauge chosen when the differential equations for the potentials are derived. For example the Lorentz gauge

$$\underline{\nabla} \cdot \underline{A} = -j\omega\mu\epsilon\Phi \quad (2.5)$$

with (2.1) and (2.2) substituted into Maxwell's equation $\underline{\nabla} \times \underline{H} = \underline{J} + j\omega\epsilon\underline{E}$, results in a set of decoupled potential equations

$$\nabla^2 \underline{A} + k^2 \underline{A} = -\mu \underline{J} \quad (2.6)$$

$$\nabla^2 \Phi + k^2 \Phi = \frac{\underline{\nabla} \cdot \underline{J}}{j\omega\epsilon} \quad (2.7)$$

where $k^2 = \omega^2\mu\epsilon$. Equation (2.6) motivates the dyadic Green's function equation

$$\nabla^2 \underline{\underline{G}}_A + k^2 \underline{\underline{G}}_A = -\underline{\underline{\delta}}(\underline{r} - \underline{r}') \quad (2.8)$$

where $\underline{\underline{\delta}} = \underline{I}\delta(\underline{r} - \underline{r}')$. $\underline{I} = \hat{x}\hat{x} + \hat{y}\hat{y} + \hat{z}\hat{z}$ is the identity dyadic and $\delta(\underline{r} - \underline{r}')$ is the Dirac delta function. Equation (2.7) effects a similar scalar Green's function equation

$$\nabla^2 G_\Phi + k^2 G_\Phi = -\delta(\underline{r} - \underline{r}') \quad (2.9)$$

Equations (2.8) and (2.9) have familiar solutions [8]:

$$\underline{\underline{G}}_A(\underline{r}|\underline{r}') = \begin{bmatrix} 1 & 0 & 0 \\ 0 & 1 & 0 \\ 0 & 0 & 1 \end{bmatrix} \frac{e^{-jkR}}{4\pi R} = \underline{\underline{I}}G(\underline{r}|\underline{r}') \quad (2.10)$$

$$G_\Phi(\underline{r}|\underline{r}') = \frac{e^{-jkR}}{4\pi R} = G(\underline{r}|\underline{r}') \quad (2.11)$$

with $R = [(x - x')^2 + (y - y')^2 + (z - z')^2]^{\frac{1}{2}}$.

2.3 Coulomb Gauge Green's Functions in Free Space

The Coulomb gauge

$$\underline{\nabla} \cdot \underline{A} = 0 \quad (2.12)$$

with (2.1) and (2.2) leads to the set of Coulomb potential equations

$$\nabla^2 \underline{A} + k^2 \underline{A} = -\mu \underline{J} + j\omega\mu\epsilon \nabla \Phi = -\mu \underline{J}^s \quad (2.13)$$

$$\nabla^2 \Phi = \frac{1}{j\omega\epsilon} \nabla \cdot \underline{J} \quad (2.14)$$

Any vector \underline{J} can be expressed solely in terms of its solenoidal (divergenceless) \underline{J}^s and lamellar (zero curl) \underline{J}^l parts. Mathematically the properties of these two parts of a vector can be described by $\nabla \times \underline{J}^s \neq 0, \nabla \cdot \underline{J}^s = 0, \nabla \times \underline{J}^l = 0, \nabla \cdot \underline{J}^l \neq 0$. The superscript s in (2.13) designates a solenoidal current density \underline{J}^s that results when the lamellar current \underline{J}^l is removed from the total current density $\underline{J} = \underline{J}^s + \underline{J}^l$. That $\underline{J}^l = j\omega\epsilon \nabla \Phi$ can be shown by taking the divergence of (2.13) and then applying the Coulomb condition (2.12). The Green's function equations pertaining to the Coulomb potential equations (2.13) and (2.14) respectively are

$$\nabla^2 \underline{G}_A^s(\underline{r}|\underline{r}') + k^2 \underline{G}_A^s(\underline{r}|\underline{r}') = -\underline{\delta}^s(\underline{r} - \underline{r}') \quad (2.15)$$

$$\nabla^2 G_\Phi(\underline{r}|\underline{r}') = -\delta(\underline{r} - \underline{r}') \quad (2.16)$$

Notice that because the dyadic delta function $\underline{\delta}^s$ is solenoidal, the Coulomb Green's function \underline{G}_A^s must also be solenoidal.

Equation (2.16) is simply the Poisson equation for a source in free space. The solution to (2.16) is

$$G_\Phi(\underline{r}|\underline{r}') = \frac{1}{4\pi R} \quad (2.17)$$

The dyadic Green's function method for solving (2.15) is in general formatable [6] but in this particular case, where the source resides in free space, we can make some observations that will lead to a method for finding the Coulomb gauge Green's function that is understandable to those readers with a basic knowledge of dyadic vector operations.

First we observe that the solenoidal part of the Lorentz gauge vector potential Green's function is equal to the Coulomb gauge vector potential Green's function. This can be shown by first decomposing the dyadics on the left and right hand sides of (2.8) into solenoidal and lamellar parts and then equating just the solenoidal components. The result is equation (2.15).

Since the Lorentz gauge Green's function is already available (equation (2.10)) our strategy is to extract its solenoidal part. This can be done by first substituting the identity $\nabla^2 \underline{A} = \nabla \nabla \cdot \underline{A} - \nabla \times \nabla \times \underline{A}$ into a second identity [9]

$$\underline{\underline{\delta}}(\underline{r} - \underline{r}') = -\frac{\underline{I}}{4\pi} \nabla^2 \frac{1}{R} \quad (2.18)$$

to get

$$\underline{\underline{\delta}}(\underline{r} - \underline{r}') = \frac{1}{4\pi} \left[-\nabla \nabla \cdot \left(\frac{\underline{I}}{R} \right) + \nabla \times \nabla \times \left(\frac{\underline{I}}{R} \right) \right] \quad (2.19)$$

The second term on the right hand side of (2.19) is the solenoidal delta function $\underline{\underline{\delta}}^s$. Now $\underline{\underline{G}}_A^s(\underline{r}|\underline{r}')$ can be found by evaluating [10]

$$\underline{\underline{G}}_A^s(\underline{r}|\underline{r}') = \int_{v''} \underline{\underline{\delta}}^s(\underline{r} - \underline{r}'') \cdot \underline{\underline{G}}_A(\underline{r}''|\underline{r}') dv'' \quad (2.20)$$

$$= \frac{1}{4\pi} \nabla \times \nabla \times \frac{\underline{I}}{R} \int_{v''} \frac{G(\underline{r}''|\underline{r}')}{|\underline{r} - \underline{r}''|} dv'' \quad (2.21)$$

where the \underline{r}'' integration extends over all space. After some tedious integration and differentiation we find that

$$\underline{\underline{G}}_A^s(\underline{r}|\underline{r}') = \begin{bmatrix} S_{xx} & S_{xy} & S_{xz} \\ S_{yx} & S_{yy} & S_{yz} \\ S_{zx} & S_{zy} & S_{zz} \end{bmatrix} \frac{e^{-jkR}}{4\pi R} = \underline{\underline{S}}G(\underline{r}|\underline{r}') \quad (2.22)$$

with

$$\underline{\underline{S}} = \left[(1-Q)\underline{I} - (1-3Q)\frac{\underline{R}\underline{R}}{R^2} \right] \quad (2.23)$$

$$Q = \frac{1 + jkR - e^{jkR}}{(kR)^2} \quad (2.24)$$

$$\underline{R} = (x - x')\hat{x} + (y - y')\hat{y} + (z - z')\hat{z} \quad (2.25)$$

This completes our presentation of the Green's functions. The gauge invariance property of the electromagnetic field [2] insures us that the fields given by (2.1) and (2.2) are unique. The equivalent current appearing in (2.3) and (2.4) is also unique (i.e. independent of gauge) and it can be used as a basis for comparing these two gauges.

2.4 Discussion

One of the apparent delimitas of the Coulomb gauge method is that when Green's method is applied to equations (2.13) and (2.15) the resulting vector potential integral contains a solenoidal current \underline{J}^s , rather than the desired surface current \underline{J} . We can immediately resolve this problem by replacing the solenoidal current with the surface current:

$$\underline{A}(\underline{r}) = \mu \int_{v'} \underline{G}_A^s(\underline{r}|\underline{r}') \cdot \underline{J}^s(\underline{r}') dv' = \mu \int_{v'} \underline{G}_A^s(\underline{r}|\underline{r}') \cdot \underline{J}(\underline{r}') dv' \quad (2.26)$$

This can be done because solenoidal and lamellar vectors are orthogonal and since the Coulomb Green's function is solenoidal, the integration process in equation (2.26) will automatically remove the lamellar part of the surface current. We emphasize that one can only numerically solve for the surface current because the solenoidal and lamellar currents can not be numerically quantified since they contain non-physical terms that exist throughout space. By analogy this last point is illustrated with equation (2.19) where the two terms on the right hand side are respectively the lamellar and solenoidal delta functions. These terms are everywhere non-zero functions of position, but together they collapse to a delta function that is non-zero only at $\underline{r} = \underline{r}'$.

Some contrasting aspects of equations (2.10) and (2.22) clearly indicate that the Lorentz gauge has a computational advantage over the Coulomb gauge. For example the Coulomb gauge Green's function contains a fully populated dyadic coefficient matrix \underline{S} while the Lorentz gauge coefficient is simply the identity dyadic \underline{I} . This means for example that current flowing in the z-direction will produce three (x, y and z) dissimilar Coulomb vector potential components or a single (z) Lorentz vector potential component. A general bent wire scatterer solved by the method of moments MPIE technique would, for most of the moment matrix, require three calculations (a column of the \underline{S} dyadic) per matrix element with the Coulomb gauge and only one calculation with the Lorentz gauge.

On the other hand for a straight wire a Coulomb gauge analysis appears at first glance to have some advantages over the Lorentz gauge because of the simple mathematical form of the Coulomb scalar potential. Although this will not prove to be the case, we present below an MPIE analysis of a straight finite length cylinder scatterer illuminated by a plane wave because it is a simple instructive problem for comparing our gauge formulations.

2.5 Results for Wire Scatterer

A straight cylinder of radius $a \ll \lambda$ and length ℓ is illuminated by a z-polarized plane wave traveling in a direction normal to the cylinder (z-) axis. By enforcing the condition that the tangential component of the total electric field is zero on the cylinder surface one gets the MPIE

$$j\omega A_z + \frac{\partial}{\partial z}\Phi = E_z^i \quad (2.27)$$

where in the Lorentz and Coulomb gauges the potentials are

$$A_z = \frac{\mu}{2\pi} \int_{z'} I(z') \int_{\varphi'} \left\{ \begin{array}{l} G(z, z', \varphi') \\ S_{zz} G(z, z', \varphi') \end{array} \right\} d\varphi' dz' \quad ; \left\{ \begin{array}{l} \text{Lorentz} \\ \text{Coulomb} \end{array} \right\} \quad (2.28)$$

$$\Phi = \frac{j}{2\pi\omega\epsilon} \int_{z'} \frac{d}{dz'} I(z') \int_{\varphi'} \left\{ \begin{array}{l} G(z, z', \varphi') \\ \frac{1}{4\pi R} \end{array} \right\} d\varphi' dz' \quad ; \left\{ \begin{array}{l} \text{Lorentz} \\ \text{Coulomb} \end{array} \right\} \quad (2.29)$$

$R = [(z - z')^2 + 2a^2 \sin^2 \varphi']^{\frac{1}{2}}$ and E_z^i represents the incident electric field. Because it is well documented [1] we will not elaborate here on the method of moments numerical technique for computing the current on a thin cylinder scatterer except to say that in our procedure we employed 20 rectangular basis and testing functions.

Fig. 2.1 shows the current distributions on three-quarter and full wavelength thin cylinders. The solid lines depict real and imaginary parts of the current due to a Coulomb gauge formulation while the overlying triangles are from the Lorentz gauge analysis. The two results are numerically indistinguishable. The computation time difference for each of these two results was 15% in favor of the Lorentz gauge.

The far zone electric field can be found by letting $r \rightarrow \infty$ in (2.28) and (2.29) and then substituting the result into equation (2.1). The far electric field is

$$E_\theta(\underline{r}) = j\omega\mu \frac{e^{-jkR}}{r} \int_{z'} I(z') e^{jkz' \cos \theta} dz' \sin \theta \quad (2.30)$$

in both gauges. Because the currents and the far field expressions are the same, there is no difference in the far fields obtained by the two gauge formulations.

The difference in the two gauges emerges in the vector and scalar potential φ' integrations. The dyadic S_{zz} is a regular non-singular function that presents no numerical difficulties. The singularity in $G(z, z', \varphi')$ is evaluated by subtracting and adding $1/R$ as follows:

$$\int_{\varphi'} G(z, z', \varphi') d\varphi' = \frac{1}{4\pi} \int_{\varphi'=-\pi}^{\pi} \frac{e^{-jkR} - 1}{R} d\varphi' + \frac{1}{4\pi} \int_{\varphi'=-\pi}^{\pi} \frac{1}{R} d\varphi' \quad (2.31)$$

Evaluation of the Lorentz scalar potential requires both integrals on the right hand side (RHS) of (2.31) while only the second RHS integral is required for the Coulomb scalar

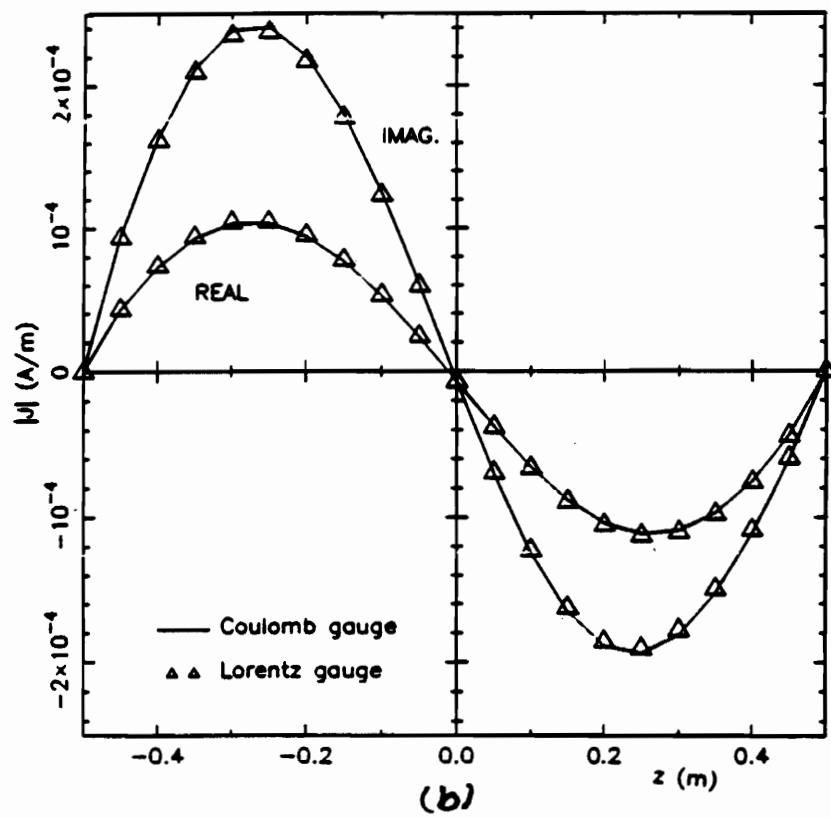
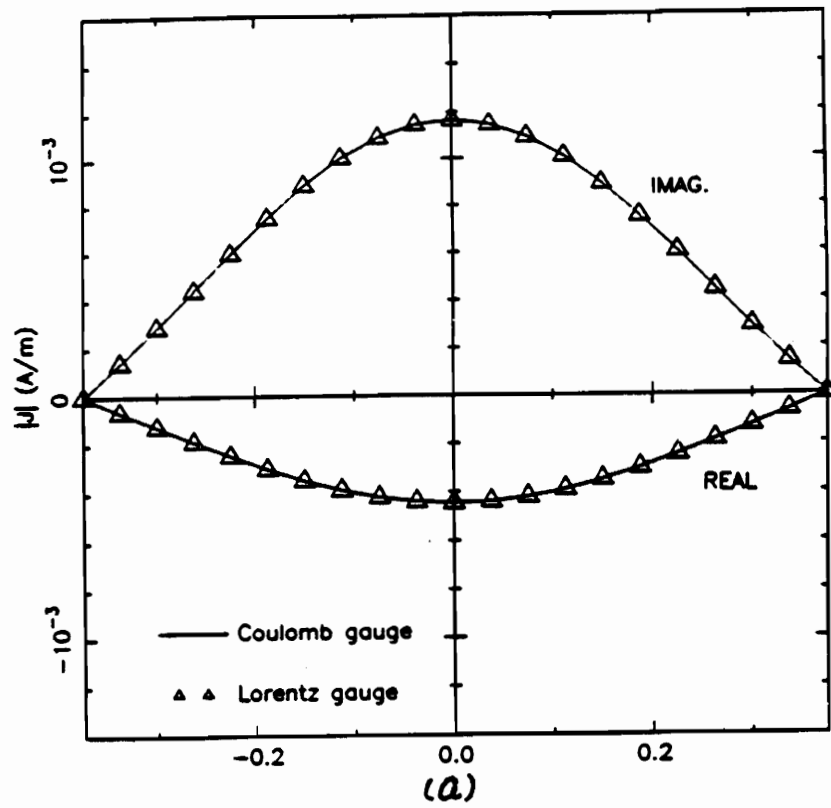


Figure 2.1: Comparison of Lorentz and Coulomb gauge current distribution on a (a) $3\lambda/4$ - dipole and a (b) λ - dipole. The incident electric field is set to unity.

potential. This advantage gained with the Coulomb gauge in the scalar potential calculation is not enough to overcome the fact that the φ' integration in the Lorentz gauge can be done once and then used in both the scalar and vector potentials (c.f. equations (2.28) and (2.29)). We can then conclude that the Lorentz gauge potentials can be computed more rapidly than the Coulomb gauge potentials for all thin wire configurations and, it is safe to say, in any case where a wire is in the presence of an object for which a Green's function can be derived.

Chapter 3

Source in a Waveguide

There are two general categories for electromagnetic boundary value problems: wave scattering and wave guidance. In this chapter we present a Coulomb gauge analysis of the fields in a source-excited waveguide. In our waveguide example the vector eigenfunction expansion method is used which is essentially the same as, but mathematically less complicated than, the wave scattering analysis found in succeeding chapters.

Historically it was thought that the scalar and vector potentials were separable only in the Lorentz gauge. However it is shown in this chapter that for perfectly conducting boundaries the scalar and vector potentials are separable in the Coulomb gauge by taking advantage of the solenoidal and lamellar properties of vectors as was done in principle for a source in infinite free space in Chapter 2.

3.1 Coulomb Gauge Vector Potential Green's Function for a Rectangular Waveguide

Consider a perfectly conducting rectangular waveguide aligned along the z -axis and with dimensions a and b along the x - and y -axes, respectively. To find $\underline{\underline{G}}_A^s$ subject to the boundary condition that $\hat{n} \times \underline{\underline{G}}_A^s = 0$ on the waveguide interior surface we follow the Ohm-Rayleigh method, as described by Tai [6]. First, we expand $\underline{\underline{\delta}}^s$ in (2.15) as follows:

$$\underline{\underline{\delta}}^s(\underline{r}|\underline{r}') = \int_{-\infty}^{\infty} dh \sum_{m=0}^{\infty} \sum_{n=0}^{\infty} \frac{2 - \delta_0}{\pi abk_c^2}$$

$$[\underline{M}_{emn}(h)\underline{M}'_{emn}(-h) + \frac{1}{\kappa^2}\underline{N}_{omn}(h)\underline{N}'_{omn}(-h)] \quad (3.1)$$

where \underline{M}_{emn} and \underline{N}_{omn} are, respectively, the even and odd solenoidal eigenfunctions of the operator $\underline{\nabla} \times \underline{\nabla} \times$, satisfying the Dirichlet boundary conditions at the waveguide walls. These vector eigenfunctions, which share the eigenvalues κ^2 , are generated by the scalar eigenfunctions $\psi_{\epsilon_{mn}}(h)$ of the operator $-\nabla^2$ according to [6]

$$\underline{M}_{\epsilon_{mn}}(h) = \underline{\nabla} \times \hat{z}\psi_{\epsilon_{mn}}(h) \quad (3.2)$$

$$\underline{N}_{\epsilon_{mn}}(h) = \underline{\nabla} \times \underline{M}_{\epsilon_{mn}}(h) \quad (3.3)$$

where ψ_{emn} and ψ_{omn} satisfy, respectively, the Neumann and Dirichlet boundary conditions at the waveguide walls. For the rectangular waveguide, one easily finds

$$\psi_{\epsilon_{mn}}(h) = \begin{cases} \cos \frac{m\pi x}{a} \cos \frac{n\pi y}{b} \\ \sin \frac{m\pi x}{a} \sin \frac{n\pi y}{b} \end{cases} e^{-jhz} \quad (3.4)$$

$$\kappa^2 = h^2 + k_c^2, \quad k_c^2 = \left(\frac{m\pi}{a}\right)^2 + \left(\frac{n\pi}{b}\right)^2 \quad (3.5)$$

The primed functions \underline{M}' and \underline{N}' in (3.1) depend on the source coordinates x', y' , and z' . The meaning of the symbol δ_0 in (3.1) is as follows: $\delta_0 = 1$ when $m = 0$ or $n = 0$ and $\delta_0 = 0$ otherwise.

With (3.1) in mind, we now expand \underline{G}_A^s as [6]

$$\underline{G}_A^s(\underline{r} | \underline{r}') = \int_{-\infty}^{\infty} dh \sum_{m=0}^{\infty} \sum_{n=0}^{\infty} \frac{2 - \delta_0}{\pi abk_c^2} \quad (3.6)$$

$$\cdot \left[a(h)\underline{M}_{emn}(h)\underline{M}'_{emn}(-h) + \frac{1}{\kappa^2}b(h)\underline{N}_{omn}(h)\underline{N}'_{omn}(-h) \right]. \quad (3.7)$$

To evaluate the coefficients $a(h)$ and $b(h)$ we substitute the expansions (3.1) and (3.7) into (2.15), introduce the operator ∇^2 under the integration and summation signs on the left side and make use of the relation $\nabla^2 \underline{M} = -\kappa^2 \underline{M}$ and a similar relation for the \underline{N} functions. As a result, we find

$$a(h) = b(h) = \frac{1}{h^2 - k_g^2} \quad (3.8)$$

where

$$k_g = \begin{cases} \sqrt{k^2 - k_c^2}, & k_c < k \\ -j\sqrt{k_c^2 - k^2}, & k_c > k. \end{cases} \quad (3.9)$$

We can now express (3.7) in the form

$$\begin{aligned} \underline{\underline{G}}_A^s(\underline{r}|\underline{r}') &= \frac{1}{k^2 ab} \sum_{m=0}^{\infty} \sum_{n=0}^{\infty} \frac{2 - \delta_0}{\pi k_c^2} \left[\int_{-\infty}^{\infty} \frac{dh}{h^2 - k_g^2} k^2 \underline{M}_{emn}(h) \underline{M}'_{emn}(-h) \right. \\ &\quad \left. + \int_{-\infty}^{\infty} \frac{dh}{h^2} \left(\frac{k_g^2}{h^2 - k_g^2} + \frac{k_c^2}{h^2 + k_c^2} \right) \underline{N}_{omn}(h) \underline{N}'_{omn}(-h) \right] \end{aligned} \quad (3.10)$$

which clearly exhibits two sets of poles in the complex h -plane, located at $\pm k_g$ and at $\pm j k_c$ ($h = 0$ is a regular point of the integrand). The integrals in (3.10) can be easily evaluated by residue calculus and the result can be expressed as

$$\underline{\underline{G}}_A^s(\underline{r}|\underline{r}') = \frac{1}{k^2} [\underline{\underline{G}}_k(\underline{r}|\underline{r}') - \underline{\underline{G}}_0(\underline{r}|\underline{r}')] \quad (3.11)$$

where

$$\underline{\underline{G}}_k(\underline{r}|\underline{r}') = \frac{1}{ab} \sum_{m=0}^{\infty} \sum_{n=0}^{\infty} \frac{2 - \delta_0}{j k_g k_c^2} [k^2 \underline{M}_{emn}(\pm k_g) \underline{M}'_{emn}(\mp k_g) \quad (3.12)$$

$$+ \underline{N}_{omn}(\pm k_g) \underline{N}'_{omn}(\mp k_g)], \quad z \gtrless z' \quad (3.13)$$

and

$$\underline{\underline{G}}_0(\underline{r}|\underline{r}') = \frac{2}{ab} \sum_{m=1}^{\infty} \sum_{n=1}^{\infty} \frac{1}{k_c^3} \underline{N}_{omn}(\mp j k_c) \underline{N}'_{omn}(\pm j k_c), \quad z \gtrless z'. \quad (3.14)$$

We observe that $\underline{\underline{G}}_0$ is the static limit of $\underline{\underline{G}}_k$, i.e.,

$$\underline{\underline{G}}_0(\underline{r}|\underline{r}') = \lim_{k \rightarrow 0} \underline{\underline{G}}_k(\underline{r}|\underline{r}'). \quad (3.15)$$

Finally, we remark that the integral in (3.1) can also be evaluated, with the result

$$\underline{\underline{\delta}}^s(\underline{r} - \underline{r}') = (\hat{x}\hat{x} + \hat{y}\hat{y})\delta(\underline{r} - \underline{r}') + \underline{\underline{G}}_0(\underline{r}|\underline{r}'). \quad (3.16)$$

3.2 Coulomb Gauge Scalar Potential Green's Function for a Rectangular Waveguide

The dyadic Green's function for the lamellar part of the electric field can be assembled in a few simple steps beginning with the solution of the static problem

$$\nabla^2 G_{\Phi}(\underline{r}|\underline{r}') = -\delta(\underline{r} - \underline{r}') \quad (3.17)$$

where G_{Φ} must vanish at the waveguide walls and at infinity.

For the rectangular waveguide, we easily find [4]

$$G_{\Phi}(\underline{r}|\underline{r}') = \frac{2}{ab} \sum_{m=1}^{\infty} \sum_{n=1}^{\infty} \frac{1}{k_c} \sin \frac{m\pi x'}{a} \sin \frac{n\pi y'}{b} \sin \frac{m\pi x}{a} \sin \frac{n\pi y}{b} e^{-k_c |z-z'|} \quad (3.18)$$

where k_c is defined in (3.5).

Finally, we observe that

$$\underline{\underline{\delta}}'(\underline{r} - \underline{r}') = \underline{\hat{z}} \underline{\hat{z}} \delta(\underline{r} - \underline{r}') - \underline{\underline{G}}_0(\underline{r}|\underline{r}'). \quad (3.19)$$

3.3 Discussion

The attractive feature of the Coulomb gauge is the explicit separation of the electric field into its lamellar and solenoidal constituents. The lamellar part, which contains the dominant R^{-3} singularity, where R is the distance between the source and the observation points, is easy to determine, since the scalar potential Φ can be obtained by a simple differentiation of the corresponding static potential. (For a few simple geometries, this potential can be obtained in closed form by image theory). The remaining part comprises the more manageable R^{-1} singularity and is, of course, solenoidal everywhere, including the source region. Hence, if the eigenfunction expansion technique is employed, \underline{E} can be conveniently represented in terms of only the solenoidal \underline{M} and \underline{N} functions, and the lamellar \underline{L} functions are indeed obviated [6].

The price paid for these advantages of the Coulomb gauge is the added difficulty in solving for the vector potential if the approach is taken of expanding \underline{A} (or \underline{E} in terms of the E and H waveguide modes [3, 11, 12]. This difficulty is due to the fact that (2.13), unlike the corresponding equation in the Lorentz gauge, involves the solenoidal part of \underline{J} which is usually a much more complicated function than \underline{J} itself. For example, \underline{J} associated with a point dipole has the simple form of the Dirac delta, whereas the corresponding \underline{J}^s and \underline{J}^l are not localized at a single point in space. These difficulties in obtaining the Coulomb vector potential can perhaps be blamed for the subtle error in Smythe's book [4], which was written years before the nature of the field in the source region was fully explored.

Chapter 4

Transverse-Electric Wave Scattering by Two-Dimensional Surfaces of Arbitrary Shape in the Presence of a Circular Cylinder

In this chapter we return to the open region problem but here we construct a hybrid MM/Green's function problem. Two forms of the MPIE are developed for two-dimensional perfectly conducting (PC) surfaces of arbitrary shape in the presence of an infinite PC cylinder of circular cross-section, subject to transverse-electric excitation. One of the MPIEs is based on the Coulomb gauge; the other employs the Lorentz gauge. In either case, the effect of the cylinder is incorporated in the integral equation by means of the appropriate Green's functions, leaving the current distribution on the arbitrary surface as the only unknown. The Green's functions are derived by the eigenfunction expansion technique. An existing well-established moment method procedure is adapted to numerically solve both forms of the MPIE. Computed results are presented for several cases.

4.1 Statement of the Problem and Assumptions

The geometry of the problem considered is shown in a cross-sectional view in Fig. 4.1, which depicts a surface S of arbitrary shape (open or closed) near a circular cylinder of radius a , whose axis coincides with the z axis of a Cartesian coordinate system (x, y, z) with an inscribed cylindrical system (ρ, φ, z) . The infinitesimally thin surface and the cylinder are made of perfect conductors and are of infinite extent and invariant along the z coordinate. The surrounding medium is homogeneous and is characterized by permittivity ϵ and permeability μ . The structure is illuminated by a plane wave transverse electric (TE) to the cylinder axis. An $e^{j\omega t}$ time convention is assumed and suppressed. The quantities of interest are the current distribution on the arbitrarily-shaped surface, the far zone field, and the bistatic radar cross-section (RCS).

4.2 Lorentz and Coulomb Gauge Green's Functions for the Cylinder

To determine $\underline{\underline{G}}_A$, we employ the eigenfunction expansion technique [6], in which the solution is sought in terms of the eigenfunctions of the vector Laplacian. These vector eigenfunctions can in turn be expressed in terms of two sets of *scalar* eigenfunctions $\psi_{n\kappa}$ and $\dot{\psi}_{n\kappa}$, which satisfy the equation

$$(\nabla_t^2 + \kappa^2) \begin{Bmatrix} \psi_{n\kappa} \\ \dot{\psi}_{n\kappa} \end{Bmatrix} = 0 \quad (4.1)$$

where ∇_t^2 is the transverse Laplacian in cylindrical coordinates, subject to, respectively, the Dirichlet and the Neumann boundary conditions at $\rho = a$. Other conditions that must also be imposed on $\psi_{n\kappa}$ and $\dot{\psi}_{n\kappa}$ are the periodicity in φ and boundedness as $\rho \rightarrow \infty$. To find $\psi_{n\kappa}$, $\dot{\psi}_{n\kappa}$ and the eigenvalues κ^2 , we follow the separation-of-variables procedure, which yields

$$\begin{Bmatrix} \psi_{n\kappa} \\ \dot{\psi}_{n\kappa} \end{Bmatrix} = \frac{e^{-jn\varphi}}{\sqrt{2\pi}} \begin{Bmatrix} J_n(\kappa\rho) + \left[\frac{\Gamma_n(\kappa a)}{\dot{\Gamma}_n(\kappa a)} \right] H_n^{(2)}(\kappa\rho) \end{Bmatrix} \quad (4.2)$$

where $n = 0, \pm 1, \pm 2, \dots$, and $0 \leq \kappa < \infty$. In the last equation, J_n and $H_n^{(2)}$ denote, respectively, the Bessel function and the Hankel function of the second kind, both of order n , and Γ_n and $\dot{\Gamma}_n$ denote the "reflection coefficients," given as

$$\Gamma_n(\kappa a) = -\frac{J_n(\kappa a)}{H_n^{(2)}(\kappa a)}, \quad \dot{\Gamma}_n(\kappa a) = -\frac{J_n'(\kappa a)}{H_n^{(2)'}(\kappa a)} \quad (4.3)$$

where J_n' and $H_n^{(2)'}$ denote derivatives with respect to the arguments of the respective functions. It can be shown that $\psi_{n\kappa}$ and $\dot{\psi}_{n\kappa}$ possess the orthogonality properties

$$\int_{-\pi}^{\pi} \int_a^{\infty} \begin{Bmatrix} \psi_{n\kappa} \\ \dot{\psi}_{n\kappa} \end{Bmatrix} \cdot \begin{Bmatrix} \psi_{n'\kappa'}^* \\ \dot{\psi}_{n'\kappa'}^* \end{Bmatrix} \rho d\rho d\varphi = \delta_{nn'} \frac{\delta(\kappa - \kappa')}{\kappa'} \quad (4.4)$$

The set of the vector eigenfunctions consists of three species [6, 13], $\underline{L}_{n\kappa}$, $\underline{M}_{n\kappa}$, and $\underline{N}_{n\kappa}$, where

$$\underline{L}_{n\kappa} = \underline{\nabla} \psi_{n\kappa} \quad (4.5)$$

$$\underline{M}_{n\kappa} = \underline{\nabla} \times \hat{z} \dot{\psi}_{n\kappa} = -\hat{z} \times \underline{\nabla} \dot{\psi}_{n\kappa} \quad (4.6)$$

and

$$\underline{N}_{n\kappa} = \frac{1}{\kappa} \underline{\nabla} \times \underline{\nabla} \times \hat{z} \psi_{n\kappa} = \hat{z} \kappa \psi_{n\kappa} \quad (4.7)$$

Clearly, the $\underline{L}_{n\kappa}$ functions are lamellar and the $\underline{M}_{n\kappa}$ and $\underline{N}_{n\kappa}$ functions are solenoidal and it can be shown that all of them satisfy (4.1). From (4.4) through (4.7), it follows that the vector eigenfunctions possess the orthogonality properties

$$\int_{-\pi}^{\pi} \int_a^{\infty} \begin{Bmatrix} \underline{L}_{n\kappa} \\ \underline{M}_{n\kappa} \\ \underline{N}_{n\kappa} \end{Bmatrix} \cdot \begin{Bmatrix} \underline{L}_{n'\kappa'}^* \\ \underline{M}_{n'\kappa'}^* \\ \underline{N}_{n'\kappa'}^* \end{Bmatrix} \rho d\rho d\varphi = \delta_{nn'} \kappa' \delta(\kappa - \kappa') \quad (4.8)$$

We now expand \underline{G}_A in (2.8) in terms of the vector eigenfunctions and invoke (4.1) and (4.8) to obtain

$$\underline{G}_A^l(\underline{\rho} | \underline{\rho}') = \sum_{n=-\infty}^{\infty} \int_0^{\infty} \frac{d\kappa}{\kappa(\kappa^2 - k^2)} \underline{L}_{n\kappa}(\underline{\rho}) \underline{L}_{n\kappa}^*(\underline{\rho}') \quad (4.9)$$

and

$$\underline{G}_A^s(\underline{\rho} | \underline{\rho}') = \sum_{n=-\infty}^{\infty} \int_0^{\infty} \frac{d\kappa}{\kappa(\kappa^2 - k^2)} [\underline{M}_{n\kappa}(\underline{\rho}) \underline{M}_{n\kappa}^*(\underline{\rho}') + \underline{N}_{n\kappa}(\underline{\rho}) \underline{N}_{n\kappa}^*(\underline{\rho}')] \quad (4.10)$$

Noting that the last term in (4.10) contributes only the $\hat{z} \hat{z}$ component of \underline{G}_A^s (which is not relevant to the TE problem considered here), we separate it by writing

$$\underline{\underline{G}}_A^s = \underline{\underline{G}}_{At}^s + \hat{z}\hat{z}G_{Azz}^s \quad (4.11)$$

where $\underline{\underline{G}}_{At}^s$ comprises only components transverse to z .

Upon substituting (4.9) into

$$\underline{\nabla} \cdot \underline{\underline{G}}_A(\underline{\rho}|\underline{\rho}') = -\underline{\nabla}' G_\Phi(\underline{\rho}|\underline{\rho}') \quad (4.12)$$

and using (4.5) and (4.1), we readily obtain the Lorentz gauge scalar potential Green's function as

$$G_\Phi(\underline{\rho}|\underline{\rho}') = \sum_{n=-\infty}^{\infty} \int_0^{\infty} \psi_{n\kappa}(\underline{\rho}) \psi_{n\kappa}^*(\underline{\rho}') \frac{\kappa d\kappa}{\kappa^2 - k^2}. \quad (4.13)$$

In view of (4.7), it immediately follows that $G_{Azz}^s = G_\Phi$.

The integrals encountered in (4.9), (4.10), and (4.13) can be evaluated by the residue calculus [13, 14]. Hence, we obtain

$$\begin{aligned} \int_0^{\infty} R_n(\kappa\rho) R_n^*(\kappa\rho') \frac{d\kappa}{\kappa(\kappa^2 - k^2)} \\ = \frac{\pi}{2jk^2} \left\{ R_n(k\rho_{<}) H_n^{(2)}(k\rho_{>}) - \frac{j}{n\pi} \left[\left(\frac{\rho_{<}}{\rho_{>}} \right)^n - \left(\frac{a^2}{\rho\rho'} \right)^n \right] \right\} \end{aligned} \quad (4.14)$$

$$\begin{aligned} \int_0^{\infty} \dot{R}_n(\kappa\rho) \dot{R}_n^*(\kappa\rho') \frac{d\kappa}{\kappa(\kappa^2 - k^2)} \\ = \frac{\pi}{2jk^2} \left\{ \dot{R}_n(k\rho_{<}) H_n^{(2)}(k\rho_{>}) - \frac{j}{n\pi} \left[\left(\frac{\rho_{<}}{\rho_{>}} \right)^n - \left(\frac{a^2}{\rho\rho'} \right)^n \right] \right\} \end{aligned} \quad (4.15)$$

and

$$\int_0^{\infty} R_n(\kappa\rho) R_n^*(\kappa\rho') \frac{\kappa d\kappa}{\kappa^2 - k^2} = \frac{\pi}{2j} R_n(k\rho_{<}) H_n^{(2)}(k\rho_{>}) \quad (4.16)$$

where $\rho_{<}$ and $\rho_{>}$ denote, respectively, the lesser and the greater of ρ and ρ' . The first right side member in each of these equations is contributed by the residue of a pole at $\kappa = k$ of the respective integrand. The remaining right side terms in (4.14)-(4.15) arise from the integration around the singularities at the origin of the κ -plane. These "static" terms have been overlooked in some past work, as pointed out in [13].

When (4.14)-(4.16) are substituted into (4.9)-(4.10) and (4.13), we expectedly find that the resulting expressions can in each case be broken into two series, of which one is analytically summable and represents the "primary" (free-space) part of the respective Green's

function, and the other, which must be summed numerically, accounts for the presence of the cylinder. We will distinguish these two parts by superscripts "p" and "c," respectively. Hence, with the notation

$$R = |\underline{\rho} - \underline{\rho}'|, \quad \xi = \varphi - \varphi' \quad (4.17)$$

$$B_1 = H_1^{(2)}(kR) - \frac{2j}{\pi kR} \quad (4.18)$$

$$B_2 = H_2^{(2)}(kR) - \frac{4j}{\pi(kR)^2} \quad (4.19)$$

we can express the primary components of \underline{G}_{At}^s as

$$G_{\rho\rho'}^{sp} = \frac{1}{4j} \left[B_1 \frac{\cos \xi}{kR} - B_2 \frac{\rho\rho'}{R^2} \sin^2 \xi \right] \quad (4.20)$$

$$G_{\rho\varphi'}^{sp} = \frac{1}{4j} \left[B_1 \frac{\sin \xi}{kR} - B_2 \frac{\rho'}{R^2} (\rho' - \rho \cos \xi) \sin \xi \right] \quad (4.21)$$

$$G_{\varphi\rho'}^{sp} = \frac{1}{4j} \left[-B_1 \frac{\sin \xi}{kR} - B_2 \frac{\rho}{R^2} (\rho - \rho' \cos \xi) \sin \xi \right] \quad (4.22)$$

$$G_{\varphi\varphi'}^{sp} = \frac{1}{4j} \left[B_1 \frac{\cos \xi}{kR} + B_2 \frac{1}{R^2} (\rho' - \rho \cos \xi)(\rho - \rho' \cos \xi) \right] \quad (4.23)$$

The remaining secondary components take the form

$$G_{\rho\rho'}^{sc} = \frac{1}{4j} \sum_{n=1}^{\infty} 2 \cos n\xi \left[\frac{n^2}{k^2 \rho\rho'} \dot{\Gamma}_n(ka) H_n^{(2)}(k\rho') H_n^{(2)}(k\rho) - Q_n \right] \quad (4.24)$$

$$G_{\rho\varphi'}^{sc} = \frac{1}{4j} \sum_{n=1}^{\infty} 2 \sin n\xi \left[\frac{n}{k\rho} \dot{\Gamma}_n(ka) H_n^{(2)'}(k\rho') H_n^{(2)}(k\rho) + Q_n \right] \quad (4.25)$$

$$G_{\varphi\rho'}^{sc} = -\frac{1}{4j} \sum_{n=1}^{\infty} 2 \sin n\xi \left[\frac{n}{k\rho'} \dot{\Gamma}_n(ka) H_n^{(2)}(k\rho') H_n^{(2)'}(k\rho) + Q_n \right] \quad (4.26)$$

$$G_{\varphi\varphi'}^{sc} = \frac{1}{4j} \sum_{n=0}^{\infty} \epsilon_n \cos n\xi \left[\dot{\Gamma}_n(ka) H_n^{(2)'}(k\rho') H_n^{(2)'}(k\rho) - Q_n \right] \quad (4.27)$$

where $\epsilon_n = 1$ for $n = 0$ and $\epsilon_n = 2$ for $n > 0$ (Neumann's number), and

$$Q_n = \frac{jn}{\pi(ka)^2} \left(\frac{a^2}{\rho\rho'} \right)^{n+1} \quad (4.28)$$

This last factor, as well as the second right side members in (4.18)-(4.19), are the previously mentioned static terms.

Finally, the primary and secondary parts of the Coulomb scalar potential Green's function G_{Φ} are found in closed form as ([15], p. 69)

$$G_{\Phi}^p = -\frac{1}{2\pi} \ln R \quad (4.29)$$

$$G_{\Phi}^c = \frac{1}{2\pi} \ln \left(\frac{\rho'}{a} |\underline{\rho} - \underline{\rho}''| \right), \quad \underline{\rho}'' = \underline{\hat{\rho}}' \frac{a^2}{\rho'} \quad (4.30)$$

Observe that, although we are solving a time-harmonic problem, this Green's function is "static," *i.e.*, it does not incorporate the time retardation effect. This paradox is characteristic of the Coulomb gauge [16].

We can obtain the lamellar part of the vector potential Green's function by a procedure analogous to that followed above for the solenoidal part. Adding the so-obtained \underline{G}'_A to the previously found \underline{G}^s_A results in the Lorentz vector potential Green's function \underline{G}_A , which we also decompose into the sum of the primary part \underline{G}^p_A and the secondary part \underline{G}^c_A . The transverse components of the former are found as

$$G_{\rho\rho'}^p = G_{\varphi\varphi'}^p = \frac{1}{4j} H_0^{(2)}(kR) \cos \xi \quad (4.31)$$

$$G_{\rho\varphi'}^p = -G_{\varphi\rho'}^p = \frac{1}{4j} H_0^{(2)}(kR) \sin \xi \quad (4.32)$$

while the corresponding components of the latter are given as

$$\begin{aligned} G_{\rho\rho'}^c = \frac{1}{4j} \sum_{n=0}^{\infty} \epsilon_n \cos n\xi \left[\Gamma_n(ka) H_n^{(2)'}(k\rho') H_n^{(2)'}(k\rho) \right. \\ \left. + \frac{n^2}{k^2 \rho\rho'} \dot{\Gamma}_n(ka) H_n^{(2)}(k\rho') H_n(k\rho) \right] \end{aligned} \quad (4.33)$$

$$\begin{aligned} G_{\rho\varphi'}^c = \frac{1}{4j} \sum_{n=1}^{\infty} 2 \sin n\xi \left[\frac{n}{k\rho'} \Gamma_n(ka) H_n^{(2)}(k\rho') H_n^{(2)'}(k\rho) \right. \\ \left. + \frac{n}{k\rho} \dot{\Gamma}_n(ka) H_n^{(2)'}(k\rho') H_n^{(2)}(k\rho) \right] \end{aligned} \quad (4.34)$$

$$\begin{aligned} G_{\varphi\rho'}^c = -\frac{1}{4j} \sum_{n=1}^{\infty} 2 \sin n\xi \left[\frac{n}{k\rho} \Gamma_n(ka) H_n^{(2)'}(k\rho') H_n^{(2)}(k\rho) \right. \\ \left. + \frac{n}{k\rho'} \dot{\Gamma}_n(ka) H_n^{(2)}(k\rho') H_n^{(2)'}(k\rho) \right] \end{aligned} \quad (4.35)$$

$$G_{\varphi\varphi'}^c = \frac{1}{4j} \sum_{n=0}^{\infty} \epsilon_n \cos n\xi \left[\frac{n^2}{k^2 \rho \rho'} \Gamma_n(ka) H_n^{(2)}(k\rho') H_n^{(2)}(k\rho) + \dot{\Gamma}_n(ka) H_n^{(2)'}(k\rho') H_n^{(2)'}(k\rho) \right] \quad (4.36)$$

It turns out that the static terms of \underline{G}_A^s and \underline{G}_A^l cancel when these dyadics are added to form \underline{G}_A , which was previously observed in [17].

Upon substituting (4.16) into (4.13), we also readily find the primary and secondary parts of the Lorentz scalar potential Green's function G_Φ as

$$G_\Phi^p = \frac{1}{4j} H_0^{(2)}(kR) \quad (4.37)$$

$$G_\Phi^c = \frac{1}{4j} \sum_{n=0}^{\infty} \epsilon_n \cos n\xi \Gamma_n(ka) H_n^{(2)}(k\rho') H_n^{(2)}(k\rho) \quad (4.38)$$

4.3 Comments

We observe that the primary terms (4.31)-(4.32) of the Lorentz gauge Green's function are much simpler than the corresponding terms (4.20)-(4.23) of its Coulomb gauge counterpart. Also, which is perhaps not obvious, the diagonal ($\rho\rho'$ and $\varphi\varphi'$) primary components of the latter exhibit a logarithmic singularity as $R \rightarrow 0$, whereas the off diagonal ($\rho\varphi'$ and $\varphi\rho'$) components are well-behaved there. (The same is clearly true about the Lorentz gauge vector potential Green's function). We note that were it not for the static terms (the second right side members in (4.18)-(4.19)), $G_{\rho\rho'}^{sp}$, and $G_{\varphi\varphi'}^{sp}$, would have nonintegrable singularities at the source point.

The static terms Q_n also help the convergence of the series (4.24)-(4.27), which would otherwise diverge. However, even with this help, the large- n behavior of the terms of these series is $O(n^0)$. In contrast, the terms of the corresponding Lorentz gauge series (4.33)-(4.36) behave as $O(n^{-1})$ for large n —which is better, but not good enough. Consequently, the series of both formulations were accelerated by Kummer's transformation ([18], p. 16), resulting in series with terms behaving as $O(n^{-2})$. Because this procedure has now become standard ([10], p. 819, [19], [20]), we omit the details here.

Finally, we remark that there are two procedures that one could follow to derive the dyadic Green's functions for the problem of Fig. 4.1 — the so-called scattering superposition

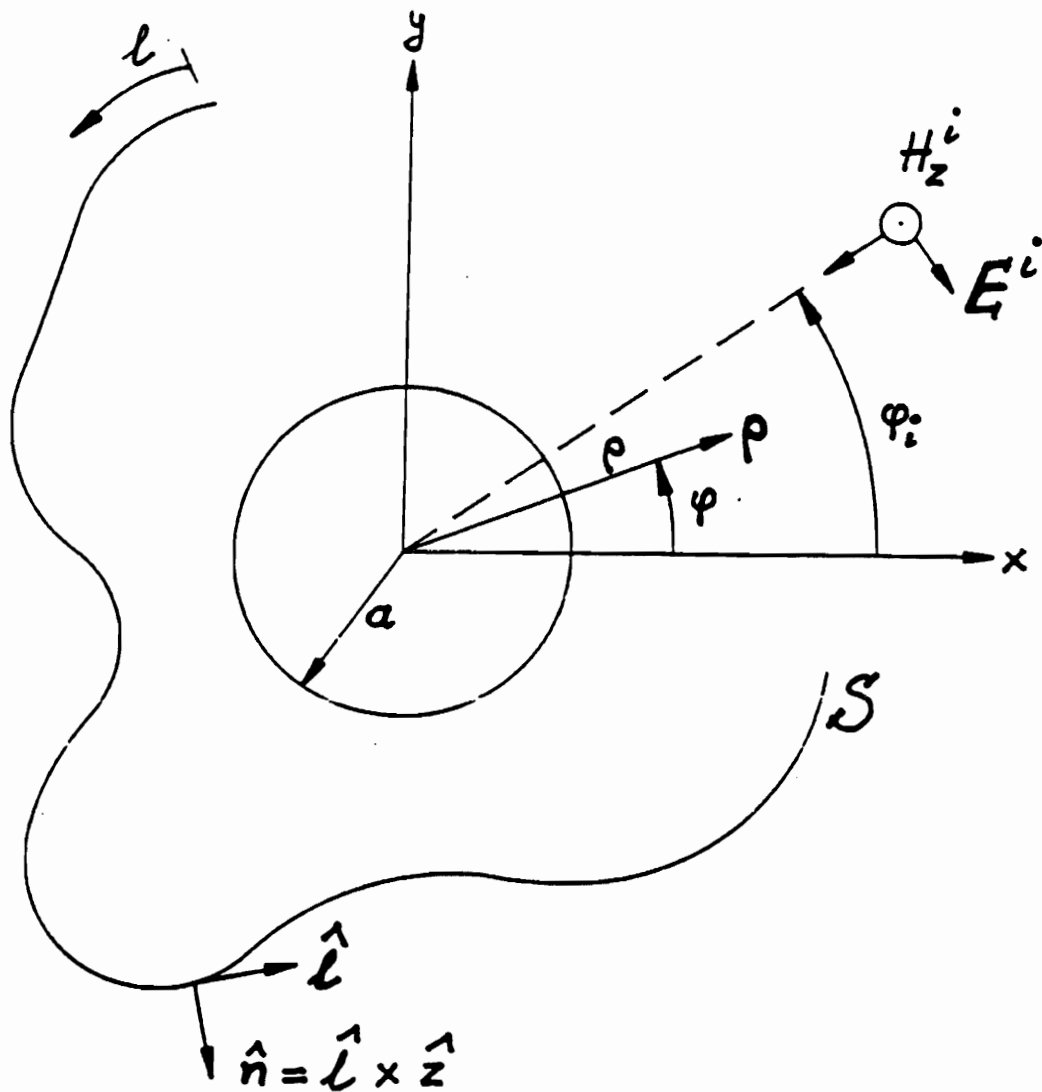


Figure 4.1: An arbitrary surface S in the presence of a circular cylinder illuminated by a TE plane wave.

method described in [6] and the method of direct eigenfunctions [17], which from the outset incorporates the effect of the cylinder. We have chosen to present the latter approach here, because we had difficulty justifying the scattering superposition technique when the static terms are present.

4.4 Numerical Method

To numerically solve the MPIEs in both gauges, we adapt the MM procedure developed in [21] for objects in free space. In this approach, the arbitrary surface is modeled in terms of straight line segments, and piece-wise linear expansion functions (*i.e.*, triangle functions which span two adjacent segments) are employed to approximate the current. The same functions are used to “test” the integral equation, producing an algebraic system of equations, which is readily solved for the current expansion coefficients. The procedure given in [21] had to be properly modified to account for the dyadic nature of the vector potential Green’s functions. We omit the details in the interest of brevity.

4.5 Scattered Far Fields

The “incident” field due to a TE plane wave with the amplitude E_0^i can be easily found ([22], p. 235) and is not listed here for the sake of brevity.

The far zone magnetic field can be found by using either the Lorentz or the Coulomb vector potential in (2.2) and letting $\rho \rightarrow \infty$. The result is

$$H_z^{\text{FAR}} = H_0^i \sqrt{\frac{2j}{\pi k \rho}} e^{-jk\rho} \left\{ \frac{k}{4H_0^i} \int_S \underline{F}^p(\rho', \varphi - \varphi') \cdot \underline{J}(\rho') dl' + \frac{k}{4H_0^i} \int_S \underline{F}^c(\rho', \varphi - \varphi') \cdot \underline{J}(\rho') dl' + P(\varphi - \varphi_i) \right\} \quad (4.39)$$

with $H_0^i = E_0^i/\eta$, where η is the intrinsic impedance of the medium.

The remaining terms in (4.39) are defined as

$$\underline{F}^p(\rho', \xi) = (\hat{\rho}' \sin \xi - \hat{\varphi}' \cos \xi) e^{jk\rho' \cos \xi} \quad (4.40)$$

$$\begin{aligned} \underline{F}^c(\rho', \xi) = & \underline{\hat{\rho}}' \sum_{n=1}^{\infty} j^{n-1} \frac{2n}{k\rho'} \dot{\Gamma}_n(ka) H_n^{(2)}(k\rho') \sin n\xi \\ & + \underline{\hat{\varphi}}' \sum_{n=0}^{\infty} \epsilon_n j^{n+1} \dot{\Gamma}_n(ka) H_n^{(2)'}(k\rho') \cos n\xi \end{aligned} \quad (4.41)$$

$$P(\xi) = \sum_{n=0}^{\infty} \epsilon_n (-1)^n \dot{\Gamma}_n(ka) \cos n\xi \quad (4.42)$$

The first and the second terms in the curly brackets in (4.39) represent, respectively, the “direct” and the “reflected” (by the cylinder) parts of the far field produced by the current \underline{J} on S , while the last term is the far zone “reflected” field produced by the incident wave.

Finally, the bistatic RCS σ is defined as ([22], p. 358)

$$\frac{\sigma}{\lambda} = k\rho \frac{|H_z^{\text{FAR}}|^2}{|H_0^i|^2} \quad (4.43)$$

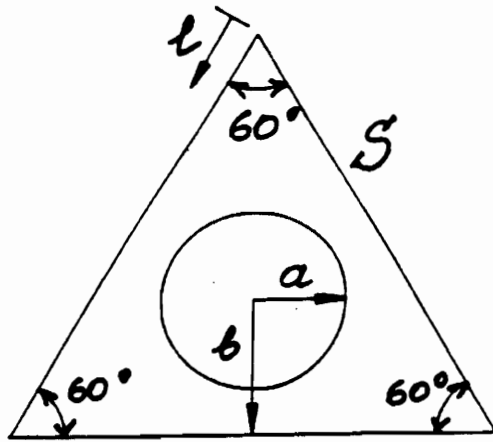
and is only a function of φ and φ_i .

4.6 Validation and Sample Results

We present in this section sample numerical results for the structures illustrated in Fig. 4.2. These simple structures have been chosen for analysis to validate the computer programs based on the Lorentz and Coulomb gauges and to compare their efficiency.

In all four cases shown in Fig. 4.2 the cylinder radius $a = 0.25\lambda$ ($ka = \pi/2$), with $\lambda = 1$ m. In the problem of Fig. 4.2(a) the cylinder resides at the center of an equilateral triangular box and is completely shielded from the incident field. Therefore, its presence is irrelevant to the exterior scattering problem, and we may compare our results with that obtained for the *empty* triangular box by a free space code [21]. Thus, in Figs. 4.3(a) and 4.3(b) are shown, respectively, the current distribution on the triangular box and the bistatic RCS (4.43) for $\varphi_i = 90^\circ$, obtained by both methods. Good agreement between the corresponding results is observed. Because the Coulomb and Lorentz gauge based programs produced graphically indistinguishable results, only the Lorentz gauge data are displayed for this and other case discussed here.

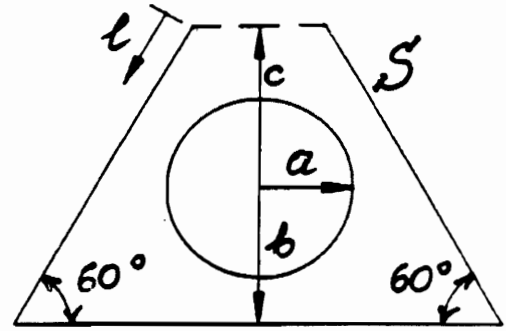
It is of interest to note that for the geometry of Fig. 4.2(a) the last two terms of (4.39) must cancel each other, because the far field is completely specified by the first right side term. When the computed approximate \underline{J} is used in (4.39), this cancellation is not perfect,



$$a = 0.25\lambda$$

$$b = 0.3\lambda$$

(a)

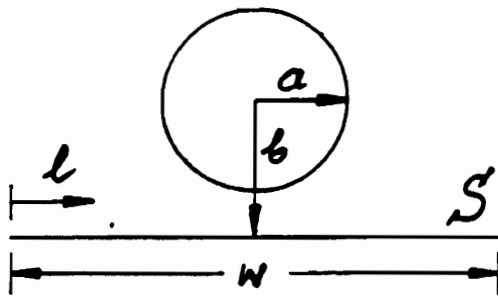


$$a = 0.25\lambda$$

$$b = 0.3\lambda$$

$$c = 0.4\lambda$$

(b)

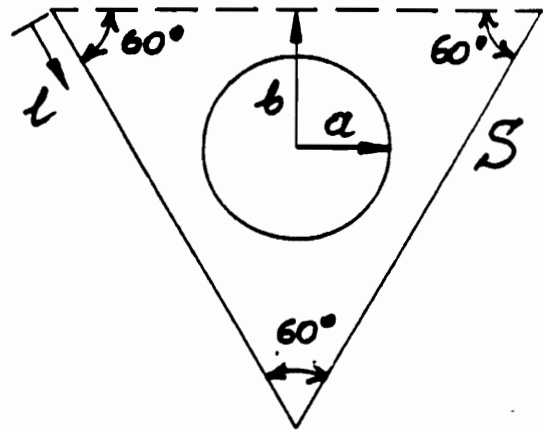


$$a = 0.25\lambda$$

$$b = 0.3\lambda$$

$$W \cong 1.04\lambda$$

(c)



$$a = 0.25\lambda$$

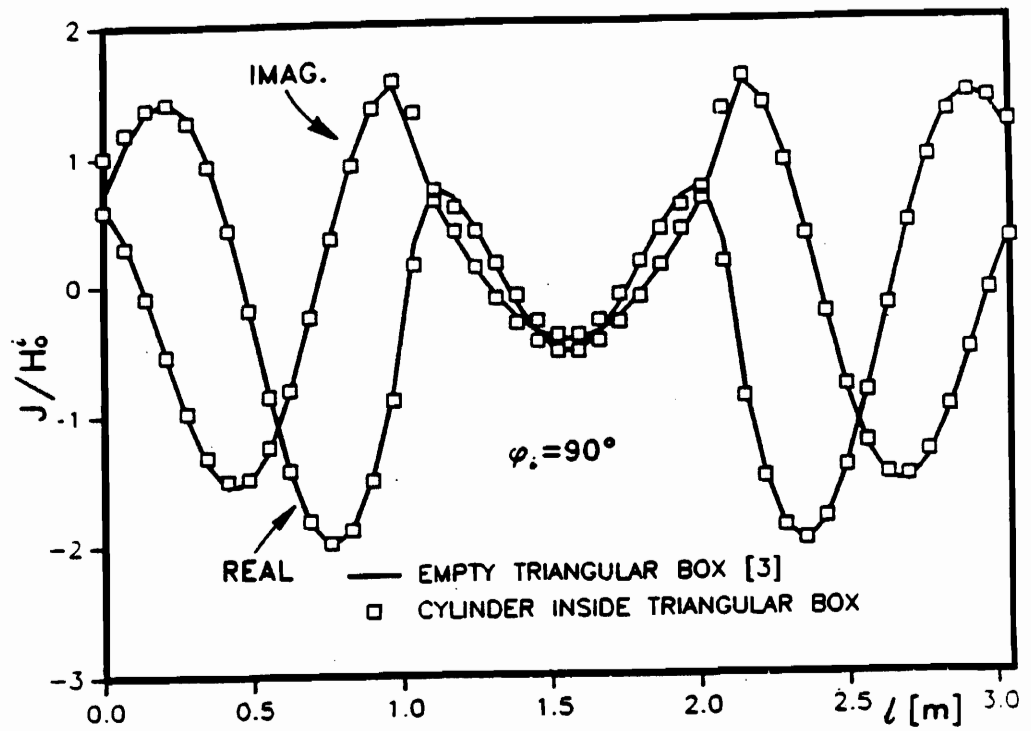
$$b = 0.3\lambda$$

(d)

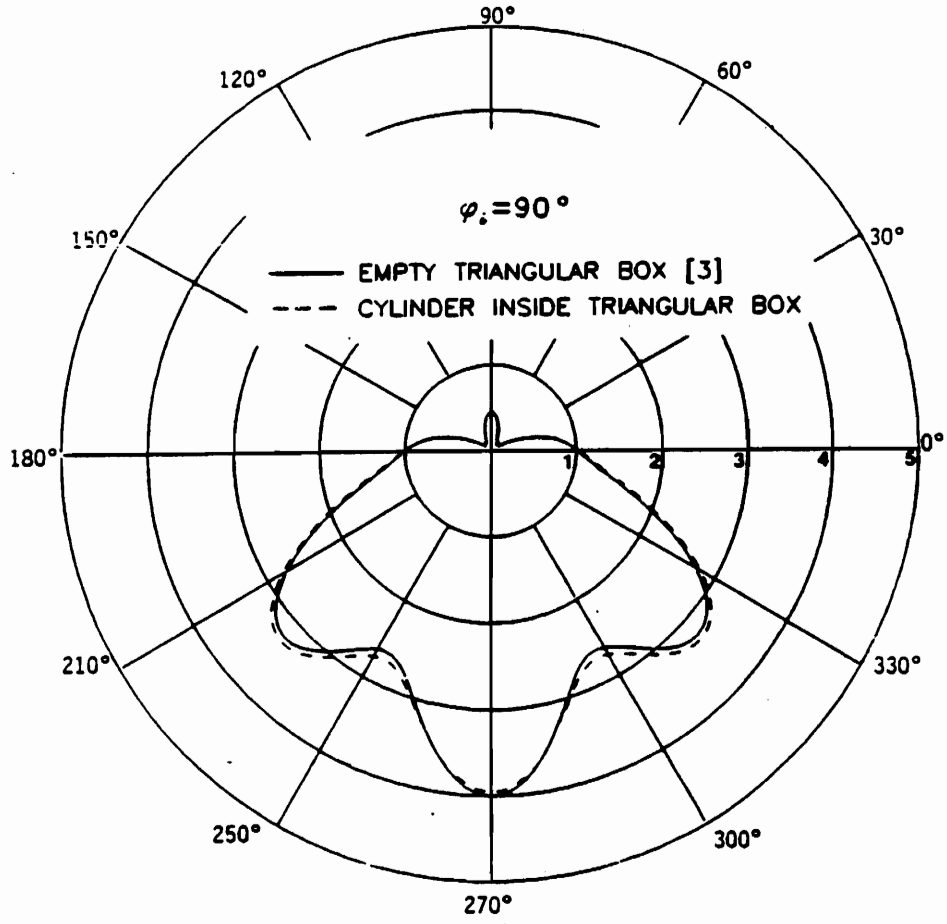
Figure 4.2: A test problem in which the surface S of Fig. 4.1 forms a triangular box enclosing the cylinder. (b)-(d) Variations of (a) in which parts of the triangular shield are removed. In all cases $\lambda = 1\text{m}$.

which is the likely reason behind the slight discrepancy in the RCS results observed in Fig. 4.3(b).

The remaining structures, illustrated in Figs. 4.2(b) through 4.2(d), are variations on the first problem. The corresponding results for two angles of incidence, $\varphi_i = 60^\circ$ and 90° , shown in Figs. 4.4 through 4.6, illustrate the effect of removing parts of the triangular shield on the current distribution and the RCS. In these examples, a 15% savings in the matrix fill time was realized when the Coulomb gauge was used instead of the Lorentz gauge.



(a)



(b)

Figure 4.3: Normalized current density on the triangular box of Fig. 4.2(a) and (b) bistatic RCS for $\varphi_i = 90^\circ$. Our results are compared with that obtained for the *empty* box by a free space code [21].

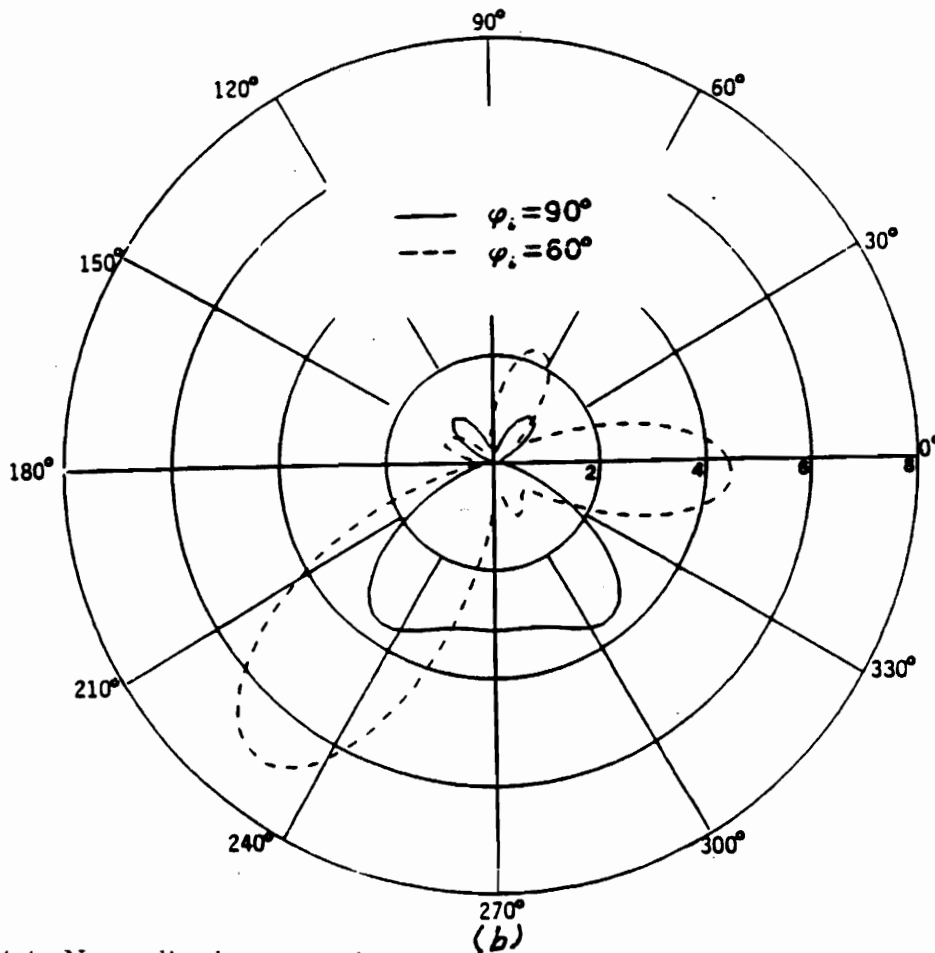
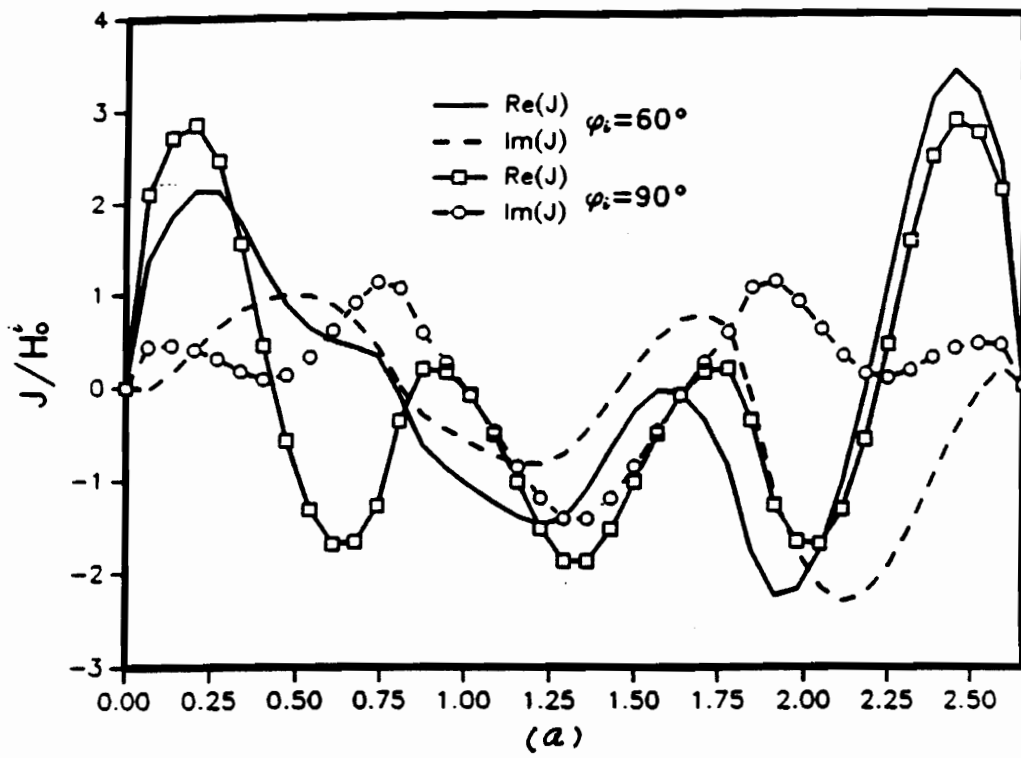


Figure 4.4: Normalized current density on S and (b) bistatic RCS for the configuration of Fig. 4.2(b) with $\varphi_i = 60^\circ$ and 90° .

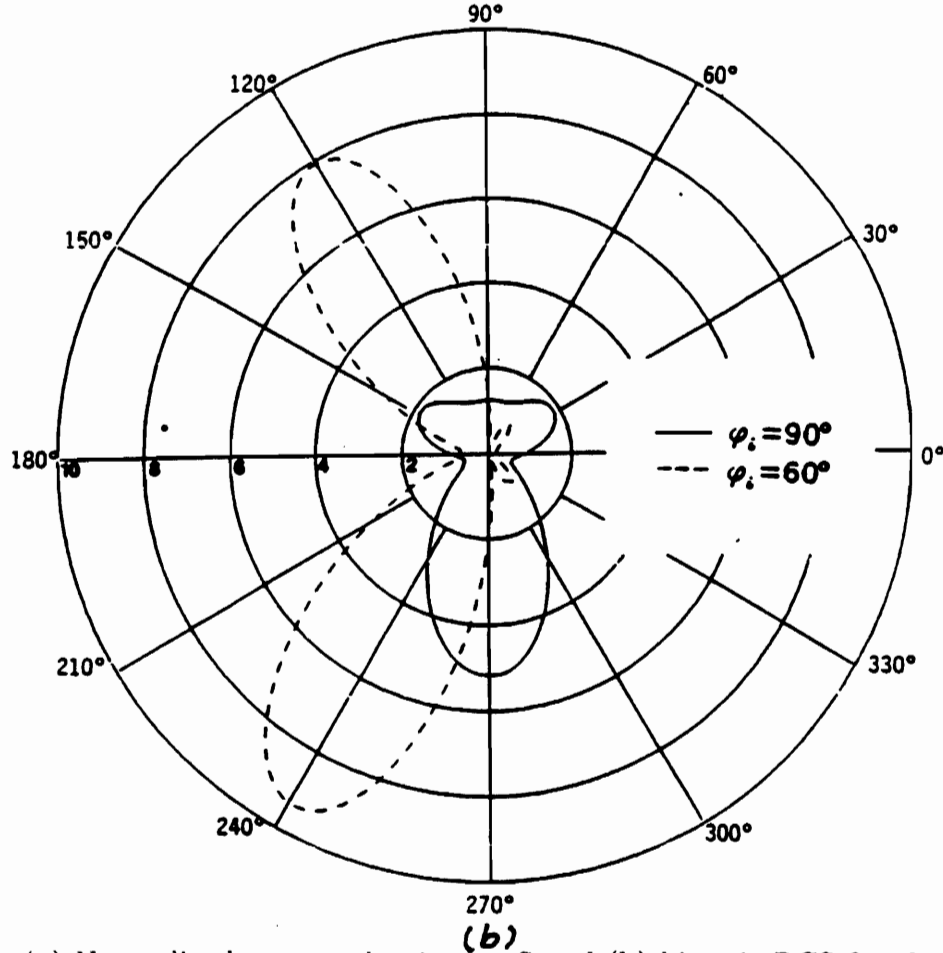
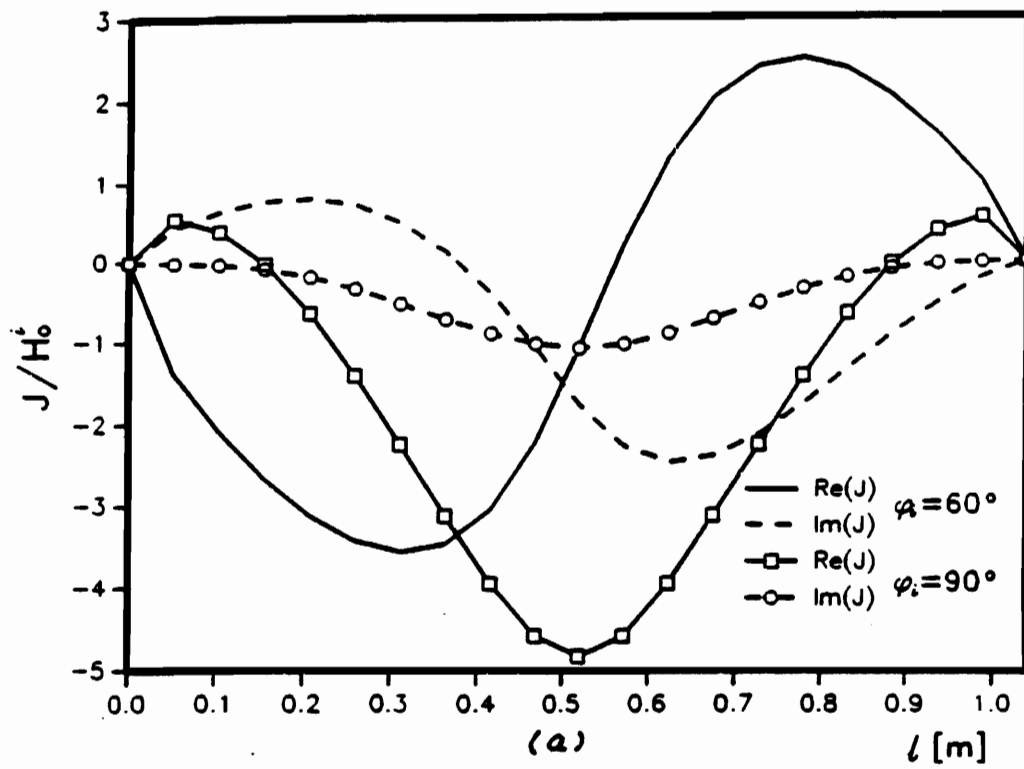


Figure 4.5: (a) Normalized current density on S and (b) bistatic RCS for the configuration of Fig. 4.2(c) with $\varphi_i = 60^\circ$ and 90° .

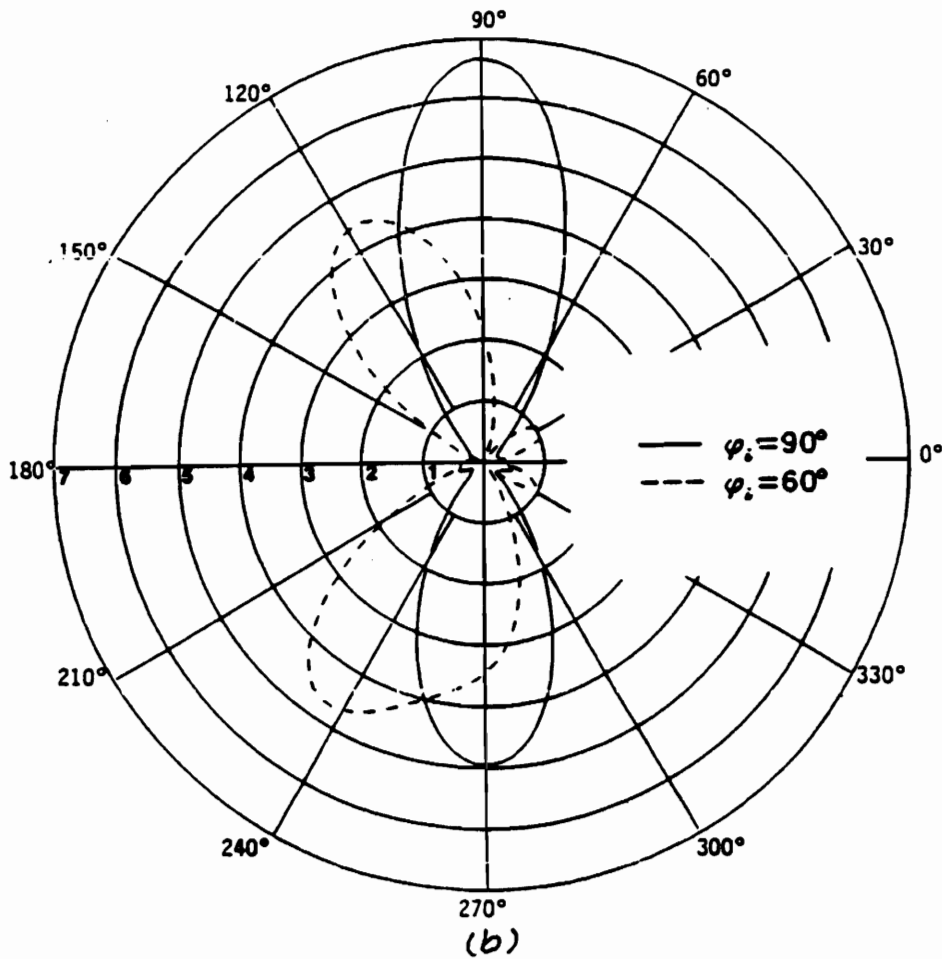
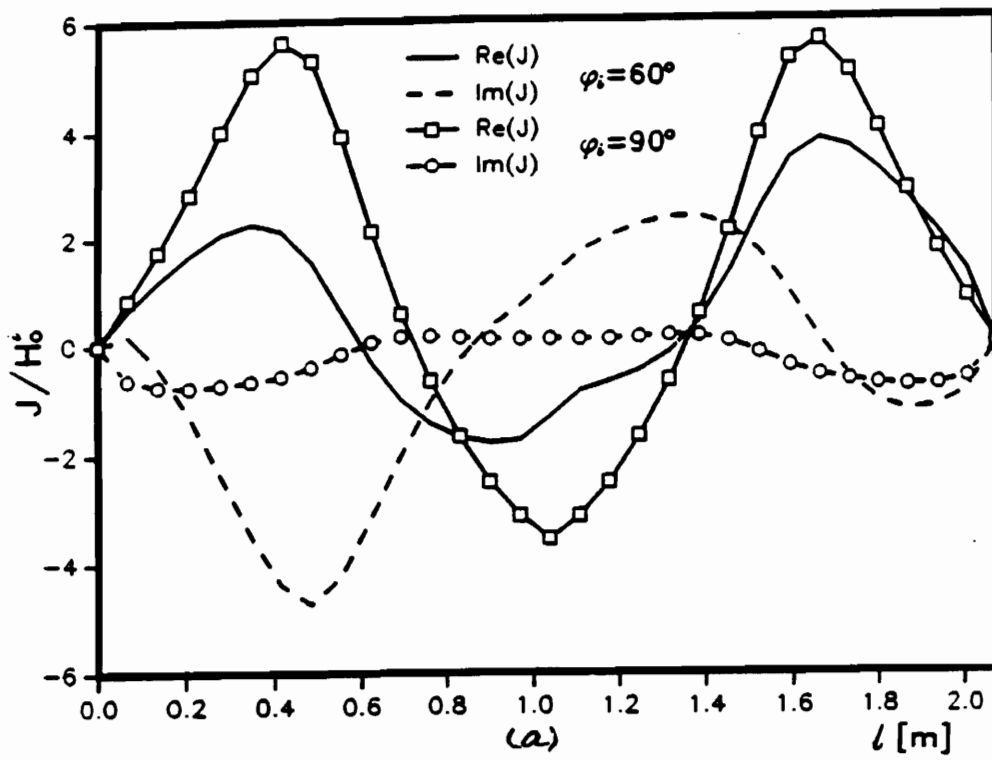


Figure 4.6: (a) Normalized current density on S and (b) bistatic RCS for the configuration of Fig. 4.2(d) with $\varphi_i = 60^\circ$ and 90° .

Chapter 5

Transverse-Electric Wave Scattering by Two-Dimensional Surfaces of Arbitrary Shape in the Presence of a Wedge

Here we investigate an infinitesimally thin, perfectly conducting (PC) surface, which is of infinite extent and invariant along the z axis, but has an arbitrary (open or closed) cross-sectional profile C , and which resides near the edge of an infinite, PC wedge of angle α , whose upper surface coincides with the $(x \geq 0, y = 0)$ half-plane (see Fig. 5.1). The surrounding medium is homogeneous and is characterized by permittivity ϵ and permeability μ . The structure is illuminated by a plane wave transverse electric (TE) to the z axis. We consider scattering from a wedge because it is one of the canonical problems of classical field theory.

5.1 The Wedge MPIE

In the case considered here (Fig. 5.1), \underline{J} is the unknown current induced on the PC surface C by a known “incident” field $\underline{E}^i, \underline{H}^i$, which exists in the presence of the wedge. Enforcing the condition that the tangential components of \underline{E} and \underline{E}^i cancel on C leads to the EFIE

$$\hat{\mathbf{t}} \times (j\omega \underline{A} + \underline{\nabla}\Phi) = \hat{\mathbf{t}} \times \underline{E}^i, \quad \rho \in C \quad (5.1)$$

where $\hat{\underline{t}}$ is a unit vector normal to C at $\underline{\rho}$. This equation is then solved for \underline{J} by the MM procedure.

5.2 Lorentz and Coulomb Gauge Green's Functions for a Wedge

We begin by constructing two scalar eigenfunctions, $\psi_{n\kappa}$ and $\dot{\psi}_{n\kappa}$, which satisfy the equation

$$(\nabla_t^2 + \kappa^2) \begin{Bmatrix} \psi_{n\kappa}(\underline{\rho}) \\ \dot{\psi}_{n\kappa}(\underline{\rho}) \end{Bmatrix} = 0 \quad (5.2)$$

subject to, respectively, the Dirichlet and Neumann boundary conditions on the PC wedge. They must also satisfy the edge condition and be bounded as $\rho \rightarrow \infty$. (In (5.2), ∇_t^2 is the transverse Laplacian in cylindrical coordinates (no z dependence).) These eigenfunctions are easily obtained by, for example, the characteristic Green's function procedure [23]. For the problem of Fig. 5.2, the normalized eigenfunctions are

$$\begin{Bmatrix} \psi_{n\kappa}(\underline{\rho}) \\ \dot{\psi}_{n\kappa}(\underline{\rho}) \end{Bmatrix} = \sqrt{\frac{\epsilon_n}{\beta}} J_{\nu_n}(\kappa\rho) \begin{Bmatrix} \sin \nu_n \varphi \\ \cos \nu_n \varphi \end{Bmatrix} \quad (5.3)$$

where ϵ_n is the Neumann number ($\epsilon_n = 1$ for $n = 0$ and $\epsilon_n = 2$ for $n > 0$), J_{ν_n} is the Bessel function of fractional order $\nu_n = n\pi/\beta$, $\beta = 2\pi - \alpha$, $0 \leq \kappa < \infty$, and $n = 0, 1, 2, \dots$. These eigenfunctions possess the orthogonality properties

$$\int_0^{\beta\infty} \int_0^{\beta\infty} \begin{Bmatrix} \psi_{n\kappa} \\ \dot{\psi}_{n\kappa} \end{Bmatrix} \begin{Bmatrix} \psi_{n'\kappa'} \\ \dot{\psi}_{n'\kappa'} \end{Bmatrix} \rho d\rho d\varphi = \delta_{nn'} \frac{\delta(\kappa - \kappa')}{\kappa'} \quad (5.4)$$

where $\delta_{nn'}$ is the Kronecker delta ($\delta_{nn'} = 1$ when $n = n'$ and zero otherwise).

We now construct three species of vector eigenfunctions, $\underline{L}_{n\kappa}$, $\underline{M}_{n\kappa}$, and $\underline{N}_{n\kappa}$, as [6,10]

$$\underline{L}_{n\kappa} = \underline{\nabla} \psi_{n\kappa} \quad (5.5)$$

$$\underline{M}_{n\kappa} = \underline{\nabla} \times \hat{\underline{z}} \dot{\psi}_{n\kappa} = -\hat{\underline{z}} \times \underline{\nabla} \dot{\psi}_{n\kappa} \quad (5.6)$$

$$\underline{N}_{n\kappa} = \frac{1}{\kappa} \underline{\nabla} \times \underline{\nabla} \times \hat{\underline{z}} \psi_{n\kappa} = \hat{\underline{z}} \kappa \psi_{n\kappa} \quad (5.7)$$

Clearly, the $\underline{L}_{n\kappa}$ functions are lamellar and the $\underline{M}_{n\kappa}$ and $\underline{N}_{n\kappa}$ functions are solenoidal. It is easily confirmed that all of them satisfy (5.2) and the required boundary conditions. It also follows from (5.4) that the vector eigenfunctions possess the orthogonality properties

$$\int_0^{\beta} \int_0^{\infty} \left\{ \begin{array}{c} \underline{L}_{n\kappa} \\ \underline{M}_{n\kappa} \\ \underline{N}_{n\kappa} \end{array} \right\} \cdot \left\{ \begin{array}{c} \underline{L}_{n'\kappa'} \\ \underline{M}_{n'\kappa'} \\ \underline{N}_{n'\kappa'} \end{array} \right\} \rho d\rho d\varphi = \delta_{nn'} \delta(\kappa - \kappa') \quad (5.8)$$

We now expand \underline{G}_A in (2.8) in terms of the vector eigenfunctions and employ (5.2) and (5.8) to obtain

$$\underline{G}_A^l(\underline{\rho} | \underline{\rho}') = \sum_{n=0}^{\infty} \int_0^{\infty} \frac{d\kappa}{\kappa(\kappa^2 - k^2)} \underline{L}_{n\kappa}(\underline{\rho}) \underline{L}_{n\kappa}(\underline{\rho}') \quad (5.9)$$

and

$$\underline{G}_A^s(\underline{\rho} | \underline{\rho}') = \sum_{n=0}^{\infty} \int_0^{\infty} \frac{d\kappa}{\kappa(\kappa^2 - k^2)} [\underline{M}_{n\kappa}(\underline{\rho}) \underline{M}_{n\kappa}(\underline{\rho}') + \underline{N}_{n\kappa}(\underline{\rho}) \underline{N}_{n\kappa}(\underline{\rho}')] \quad (5.10)$$

Noting that the term in (5.10) comprising the $\underline{N}_{n\kappa}$ functions contributes only the $\hat{z}\hat{z}$ component of \underline{G}_A^s , we separate it by writing

$$\underline{G}_A^s = \underline{G}_{At}^s + \hat{z}\hat{z}G_{Azz}^s \quad (5.11)$$

where only \underline{G}_{At}^s , the transverse part of \underline{G}_A^s , is of consequence to the TE problem considered here.

Using (5.9) in

$$\underline{\nabla} \cdot \underline{G}_A^l = -\underline{\nabla}' G_{\Phi}(\underline{\rho} | \underline{\rho}') \quad (5.12)$$

we easily find the Lorentz scalar potential Green's function as

$$G_{\Phi}(\underline{\rho} | \underline{\rho}') = \sum_{n=1}^{\infty} \int_0^{\infty} \psi_{n\kappa}(\underline{\rho}) \psi_{n\kappa}(\underline{\rho}') \frac{\kappa d\kappa}{\kappa^2 - k^2} \quad (5.13)$$

(which, incidentally, is identical with G_{Azz}^s).

The eigenfunction expansion method can also be used to solve (2.17) for the Coulomb scalar potential Green's function, with the result

$$G_{\Phi}(\underline{\rho} | \underline{\rho}') = \sum_{n=1}^{\infty} \int_0^{\infty} \psi_{n\kappa}(\underline{\rho}) \psi_{n\kappa}(\underline{\rho}') \frac{d\kappa}{\kappa} \quad (5.14)$$

The integrations over the radial spectral variable κ in (5.9)-(5.10) and in (5.11)-(5.12) can be done upon using [13]

$$\int_0^{\infty} J_{\nu}(\kappa\rho) J_{\nu}(\kappa\rho') \frac{d\kappa}{\kappa} = \frac{1}{2\nu} \left(\frac{\rho_{<}}{\rho_{>}} \right)^{\nu}, \quad \nu > 0 \quad (5.15)$$

$$\int_0^{\infty} J_{\nu}(\kappa\rho) J_{\nu}(\kappa\rho') \frac{\kappa d\kappa}{\kappa^2 - k^2} = -\frac{\pi j}{2} J_{\nu}(k\rho_{<}) H_{\nu}^{(2)}(k\rho_{>}), \quad \nu \geq 0 \quad (5.16)$$

and

$$\int_0^{\infty} J_{\nu}(\kappa\rho) J_{\nu}(\kappa\rho') \frac{d\kappa}{\kappa(\kappa^2 - k^2)} = -\frac{\pi j}{2k^2} \left[J_{\nu}(k\rho_{<}) H_{\nu}^{(2)}(k\rho_{>}) - \frac{j}{\nu\pi} \left(\frac{\rho_{<}}{\rho_{>}} \right)^{\nu} \right], \quad \nu > 0 \quad (5.17)$$

where $\rho_{>}$ denotes the greater, and $\rho_{<}$ the lesser, of ρ and ρ' , and $H_{\nu}^{(2)}$ is the Hankel function of the second kind and order ν . In the above and henceforth, we omit the subscript n on ν for notational simplicity.

Using (5.17) in (5.10) and the notation

$$c_n^{\pm} = \cos \nu(\varphi - \varphi') \pm \cos \nu(\varphi + \varphi') \quad (5.18)$$

$$s_n^{\pm} = \sin \nu(\varphi - \varphi') \pm \sin \nu(\varphi + \varphi') \quad (5.19)$$

$$b_n^{\rho\rho'} = \frac{\nu}{k^2 \rho \rho'} J_{\nu}(k\rho_{<}) H_{\nu}^{(2)}(k\rho_{>}) - \nu \Omega_n \quad (5.20)$$

$$b_n^{\rho\varphi'} = \begin{cases} \frac{\nu}{k\rho} J'_{\nu}(k\rho') H_{\nu}^{(2)}(k\rho) - \nu \Omega_n, & \rho > \rho' \\ \frac{\nu}{k\rho} J_{\nu}(k\rho) H_{\nu}^{(2)'}(k\rho') + \nu \Omega_n, & \rho < \rho' \end{cases} \quad (5.21)$$

$$b_n^{\varphi\rho'} = \begin{cases} -\frac{\nu}{k\rho'} J_{\nu}(k\rho') H_{\nu}^{(2)'}(k\rho) - \nu \Omega_n, & \rho > \rho' \\ -\frac{\nu}{k\rho'} J'_{\nu}(k\rho) H_{\nu}^{(2)}(k\rho') + \nu \Omega_n, & \rho < \rho' \end{cases} \quad (5.22)$$

$$b_n^{\varphi\varphi'} = J'_{\nu}(k\rho_{<}) H_{\nu}^{(2)'}(k\rho_{>}) + \nu \Omega_n \quad (5.23)$$

where J'_{ν} and $H_{\nu}^{(2)'}$ denote derivatives with respect to the arguments of the respective functions and

$$\Omega_n = \frac{j}{\pi k^2 \rho \rho'} \left(\frac{\rho <}{\rho >} \right)^\nu \quad (5.24)$$

we can express the elements of $\underline{\underline{G}}_{At}^s$ as

$$G_{A\rho\rho'}^s = \frac{\pi}{2j\beta} \sum_{n=1}^{\infty} c_n^- b_n^{\rho\rho'} \quad (5.25)$$

$$G_{A\rho\varphi'}^s = \frac{\pi}{2j\beta} \sum_{n=1}^{\infty} s_n^+ b_n^{\rho\varphi'} \quad (5.26)$$

$$G_{A\varphi\rho'}^s = \frac{\pi}{2j\beta} \sum_{n=1}^{\infty} s_n^- b_n^{\varphi\rho'} \quad (5.27)$$

$$G_{A\varphi\varphi'}^s = \frac{\pi}{4j\beta} \sum_{n=0}^{\infty} \epsilon_n c_n^+ b_n^{\varphi\varphi'} \quad (5.28)$$

Finally, using (5.15) in (5.14) and summing the resulting series, we can express the Coulomb scalar potential as

$$G_\Phi = -\frac{1}{2\pi} (\ln R^- - \ln R^+) \quad (5.29)$$

where

$$R^\pm = (1 - 2\xi \cos \zeta^\pm + \xi^2)^{\frac{1}{2}} \quad (5.30)$$

with

$$\zeta^\pm = \frac{\pi}{\beta} (\varphi \pm \varphi'), \quad \xi = \left(\frac{\rho <}{\rho >} \right)^{\frac{\pi}{\beta}} \quad (5.31)$$

The lamellar part of $\underline{\underline{G}}_A$ can also be transformed by a procedure analogous to that used to obtain equations (5.25)-(5.28). When the corresponding components of $\underline{\underline{G}}_A^l$ and $\underline{\underline{G}}_{At}^s$ are added to form the transverse part of the Lorentz vector potential Green's function, cancellations occur, resulting in the relatively simple expressions

$$G_{A\rho\rho'} = \frac{\pi}{2j\beta} \sum_{n=1}^{\infty} c_n^- a_n^+ \quad (5.32)$$

$$G_{A\rho\varphi'} = \frac{\pi}{2j\beta} \sum_{n=1}^{\infty} s_n^+ a_n^- \quad (5.33)$$

$$G_{A\varphi\rho'} = -\frac{\pi}{2j\beta} \sum_{n=1}^{\infty} s_n^- a_n^- \quad (5.34)$$

$$G_{A\varphi\rho'} = \frac{\pi}{4j\beta} \sum_{n=0}^{\infty} \epsilon_n c_n^+ a_n^+ \quad (5.35)$$

where

$$a_n^\pm = \frac{1}{2} \left[J_{\nu-1}(k\rho_<) H_{\nu-1}^{(2)}(k\rho_>) \pm J_{\nu+1}(k\rho_<) H_{\nu+1}^{(2)}(k\rho_>) \right] \quad (5.36)$$

Finally, using (5.16) in (5.13), we express the Lorentz scalar potential as

$$G_\Phi = \frac{\pi}{2j\beta} \sum_{n=1}^{\infty} c_n^- J_\nu(k\rho_<) H_\nu^{(2)}(k\rho_>) \quad (5.37)$$

5.3 Series Acceleration

The series in (5.25)-(5.28) are slowly convergent, which can be appreciated by examining their large- n asymptotic behavior. Hence, keeping terms up to $O(n^{-1})$, we find

$$b_n^{\rho\rho'} \sim \Omega_n \left[T_- + \frac{1}{2\nu}(T_-^2 + 2T_+) \right] \quad (5.38)$$

$$b_n^{\rho\rho'} \sim \pm \Omega_n \left[T_- + \frac{1}{2\nu} T_- (T_- \pm 2) \right] \quad (5.39)$$

$$b_n^{\varphi\rho'} \sim \pm \Omega_n \left[T_- + \frac{1}{2\nu} T_- (T_- \mp 2) \right] \quad (5.40)$$

$$b_n^{\varphi\rho'} \sim -\Omega_n \left[T_- + \frac{1}{2\nu}(T_-^2 - 2T_+) \right] \quad (5.41)$$

where the upper and lower signs correspond, respectively, to $\rho > \rho'$ and $\rho < \rho'$, and

$$T_\pm = \left(\frac{k\rho_>}{2} \right)^2 \pm \left(\frac{k\rho_<}{2} \right)^2 \quad (5.42)$$

Observe that the leading terms in (5.38)-(5.41) are $O(n^0)$. The series (5.32)-(5.35) and (5.37) of the Lorentz gauge formulation behave slightly better, which is evident from the asymptotic forms

$$a_n^\pm \sim \frac{j\xi^n}{2\nu\pi} \frac{1 \pm \left(\frac{\rho_<}{\rho_>} \right)^2}{\left(\frac{\rho_<}{\rho_>} \right)} \quad (5.43)$$

and

$$J_\nu(k\rho_<) H_\nu^{(2)}(k\rho_>) \sim \frac{j\xi^n}{\nu\pi} \quad (5.44)$$

The large- n expansions (5.38)-(5.41) and (5.43)-(5.44) have been used in conjunction with the Kummer transformation [18] to accelerate the convergence of the respective series. In this method, we subtract from each term of the series its

large- n form, which results in a more rapidly converging series. To preserve the correct value of the sum, the modified series is augmented by the series of asymptotic forms, which can be summed in closed form. The closed-form sums needed in our case are

$$\sum_{n=1}^{\infty} \frac{\xi^n}{n} \cos n\zeta^\pm = -\ln R^\pm \quad (5.45)$$

$$\sum_{n=1}^{\infty} \frac{\xi^n}{n} \sin n\zeta^\pm = \arctan \left[\frac{\xi \sin \zeta^\pm}{1 - \xi \cos \zeta^\pm} \right] \quad (5.46)$$

$$\sum_{n=1}^{\infty} \xi^n \cos n\zeta^\pm = \frac{\xi}{R^{\pm 2}} (\cos \zeta^\pm - \xi) \quad (5.47)$$

$$\sum_{n=1}^{\infty} \xi^n \sin n\zeta^\pm = \frac{\xi \sin \zeta^\pm}{R^{\pm 2}} \quad (5.48)$$

These sums are easily derivable from the geometric series [20].

After the Kummer transformation, all series have terms with large- n behavior $O(n^{-2})$, which is manageable. However, we note that more effort is required to accelerate the Coulomb gauge series than is needed to accelerate the Lorentz gauge series to the same rate of convergence. On the other hand, the scalar potential Green's function of the Coulomb formulation is available in closed form, whereas that of the Lorentz formulation is in a series form and must be summed numerically.

Finally, we note that G_Φ and the $\rho\rho'$ and $\varphi\varphi'$ terms of \underline{G}_A and \underline{G}_A^s are logarithmically singular when $\underline{\rho}$ approaches $\underline{\rho}'$. The added benefit of the Kummer transformation is the removal of the singularities from the corresponding series.

5.4 Incident Field and Far Field Pattern

The TE plane wave with amplitude E_0 impinging upon the wedge at an angle φ_i (Fig. 5.1) produces in the absence of the arbitrary scatterer C the “incident” field \underline{E}^i, H_z^i . The components of \underline{E}^i , which appear as the driving function in the integral equation (5.1), are easily found as [22]

$$E_\varphi^i = E_0 \frac{\pi}{\beta} \sum_{n=0}^{\infty} \epsilon_n e^{j(\nu+1)\pi/2} J'_\nu(k\rho) [\cos \nu(\varphi - \varphi_i) + \cos \nu(\varphi + \varphi_i)] \quad (5.49)$$

$$E_\rho^i = E_0 \frac{\pi}{\beta} \sum_{n=1}^{\infty} \frac{2\nu}{k\rho} e^{j(\nu+1)\pi/2} J_\nu(k\rho) [\sin \nu(\varphi - \varphi_i) + \sin \nu(\varphi + \varphi_i)] \quad (5.50)$$

When the scatterer is introduced near the wedge, the field \underline{E}^i, H_z^i is modified by the “scattered” field \underline{E}^s, H_z^s , whose source is the surface current (of density \underline{J}) induced on C . It can be shown that far from the edge

$$H_z^s = \left(\frac{2j}{\pi k\rho} \right)^{\frac{1}{2}} e^{-jk\rho} P(\varphi) \quad (5.51)$$

where

$$P(\varphi) = \frac{\pi k}{4\beta j} \int_C \underline{E}(\underline{\rho}', \varphi) \cdot \underline{J}(\underline{\rho}') dl' \quad (5.52)$$

is the far field pattern, in which

$$\underline{E}(\underline{\rho}', \varphi) = \underline{\hat{\rho}}' \sum_{n=1}^{\infty} \frac{2\nu}{k\rho'} s_n^- e^{j\nu\pi/2} J_\nu(k\rho') - \underline{\hat{\varphi}}' \sum_{n=0}^{\infty} \epsilon_n c_n^+ e^{j\nu\pi/2} J'_\nu(k\rho') \quad (5.53)$$

5.5 Sample Results

We present in this section sample numerical results for several simple structures near a wedge with different values of α (see Fig. 5.1). In all cases, $f = 300$ MHz, which corresponds to free-space wavelength $\lambda = 1$ m.

In Figs. 5.3(a) and 5.3(b) are shown, respectively, the current distribution and the far field pattern for an inverted rectangular trough with its ends touching a PC ground plane (which corresponds to $\alpha = 180^\circ$) under normal incidence. Our results are compared with that obtained for the trough and its image (a rectangular box) by a free space code [21],

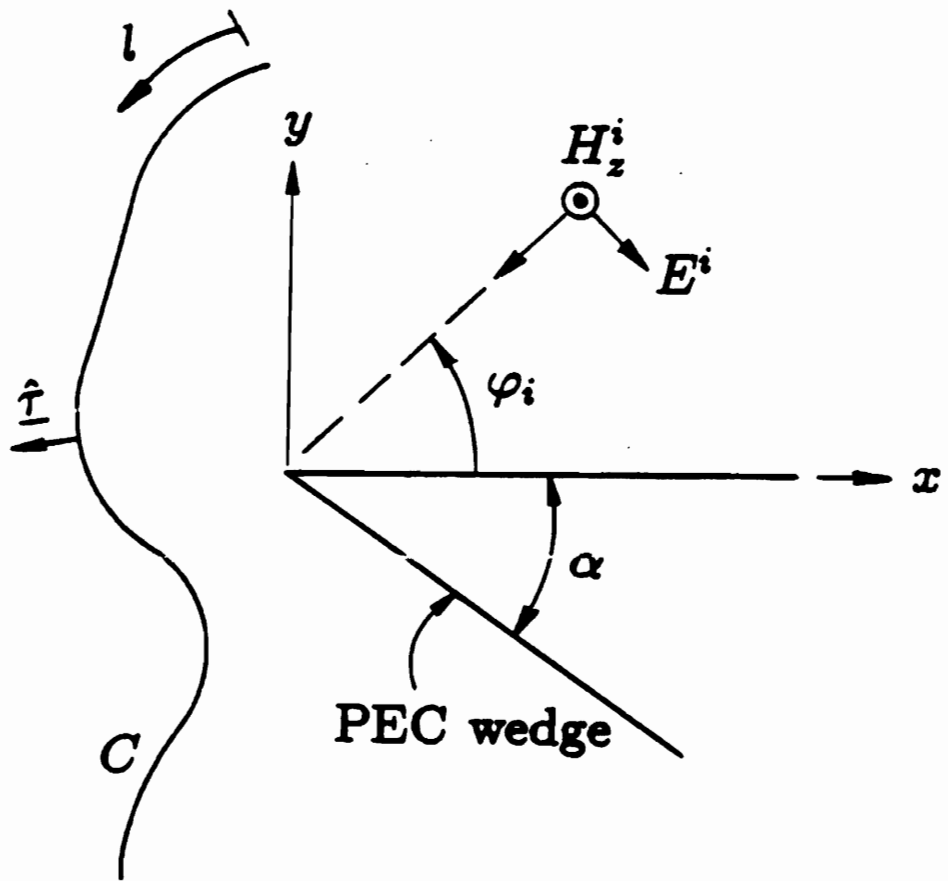


Figure 5.1: Scatterer of arbitrary cross-sectional profile C in the presence of an infinite wedge.

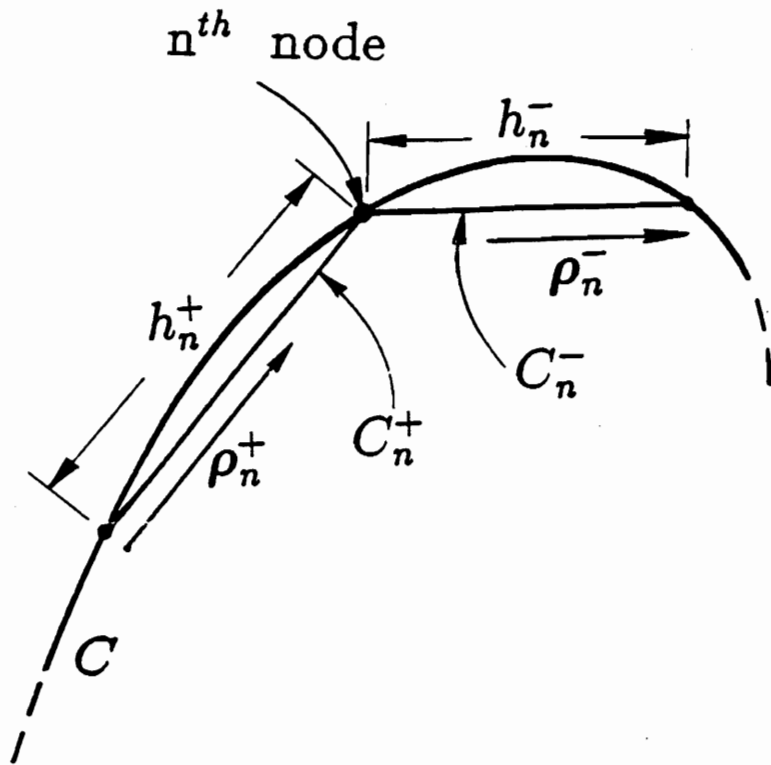


Figure 5.2: Contour C approximated by straight line segments and local coordinates associated with the n th node.

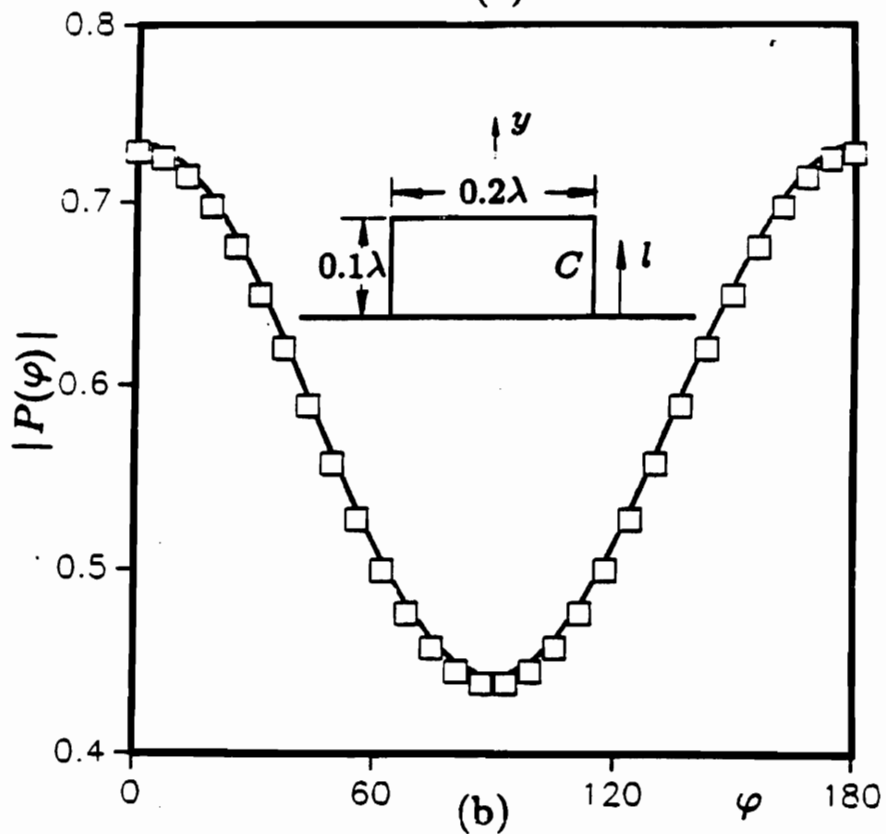
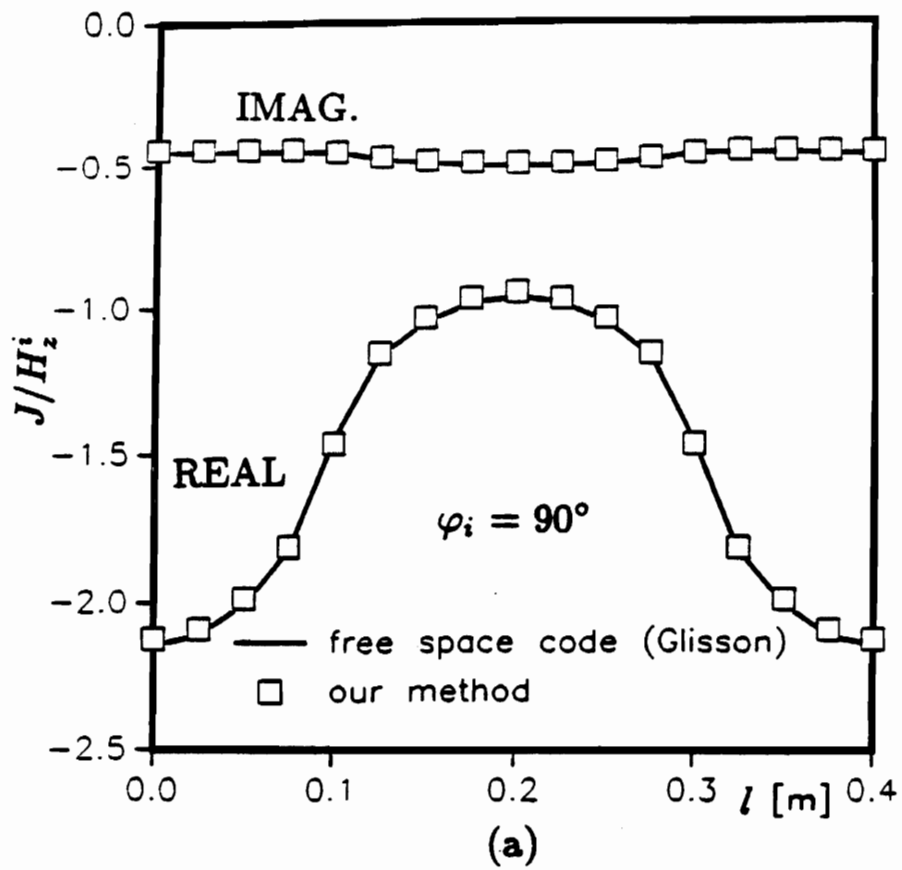


Figure 5.3: (a) Normalized current density on C and (b) far field pattern for an inverted trough on a ground plane illuminated by a normally incident plane wave.

and excellent agreement is observed. Since the Coulomb and Lorentz gauge based programs produced graphically indistinguishable results, only the Lorentz gauge data are displayed for this and other cases discussed here.

The next structure considered was that of a circular cylinder of radius $a = \lambda/2\pi$, enclosing the edge of a wedge with $\alpha = 30^\circ$, thus simulating a cylindrically tipped wedge, for which an exact solution is available [24]. The circular profile C of the cylinder was approximated by thirty straight line segments. The current distribution on C for $\varphi_i = 45^\circ$ is shown in Fig. 5.4(a) and the corresponding far field pattern in Fig. 5.4(b), where the exact result [26] is also shown for comparison. When the wedge angle α is set to zero, a cylindrically tipped half-plane is obtained. The corresponding results are shown in Figs. 5.5(a) and 5.5(b). In this case, thirty five segments were used to model the cylindrical profile C .

Finally, in Figs. 5.6(a) and 5.6(b) we present results for a half-plane ($\alpha = 0^\circ$) with the edge enclosed by a square box with the diagonal of 0.5λ , illuminated by a plane wave with $\varphi_i = 45^\circ$. Since the edge is completely shielded from the incident field, its position inside the box should have no effect on the magnitude of the induced current. This is indeed observed in Fig. 5.6(a), where one result is for a half-plane extending to the center of the box, and the other is for the case where the edge of the half-plane is displaced 0.1λ from the center of the box.

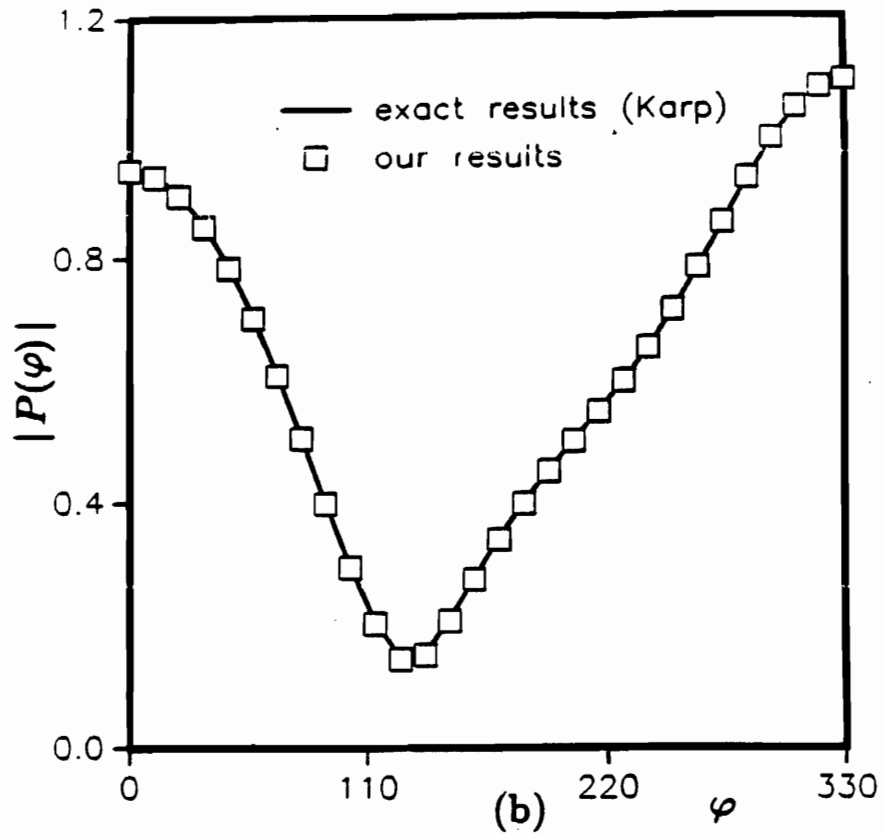
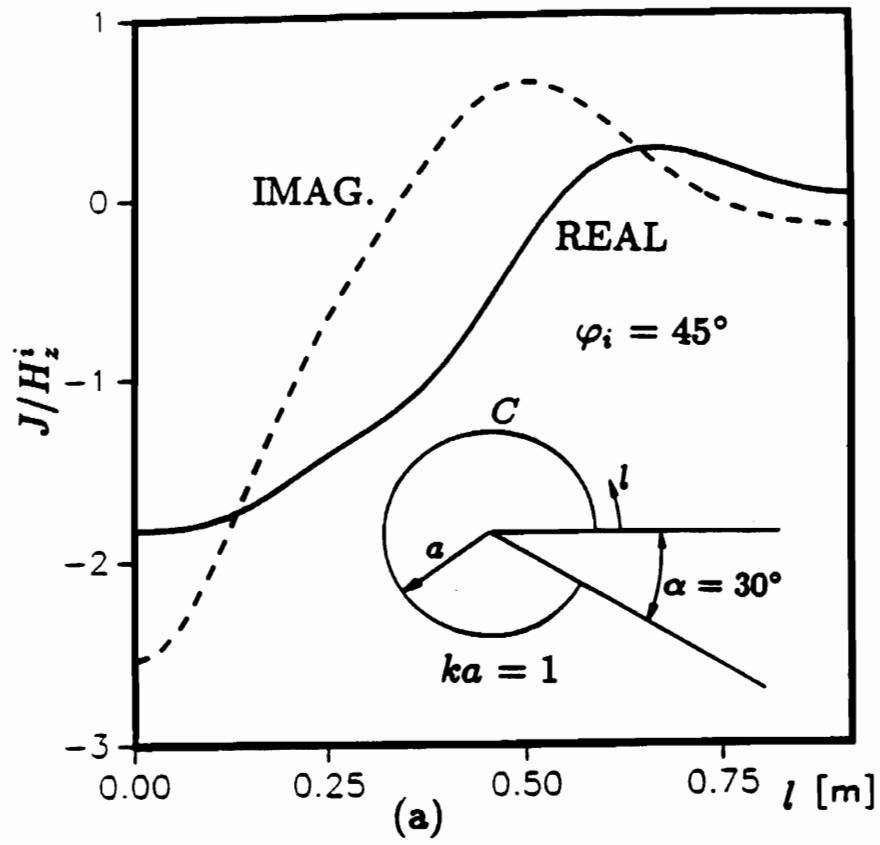


Figure 5.4: (a) Normalized current density on C and (b) far field pattern for a cylindrically tipped wedge ($\alpha = 30^\circ$) illuminated by a plane wave with $\varphi_i = 45^\circ$.

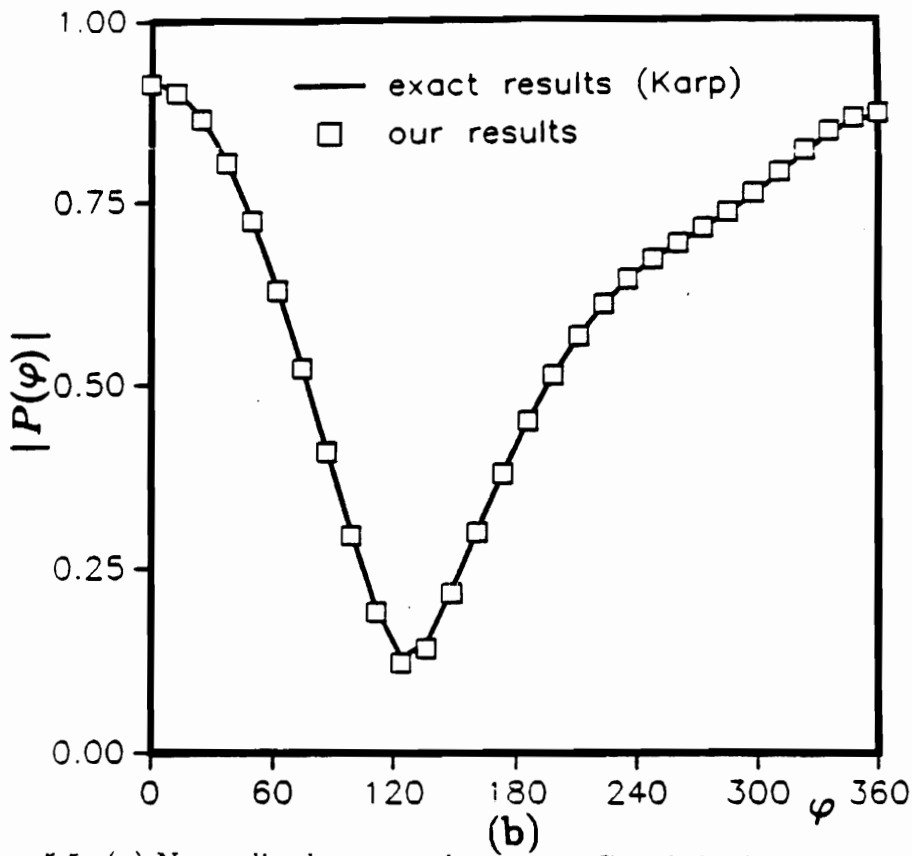
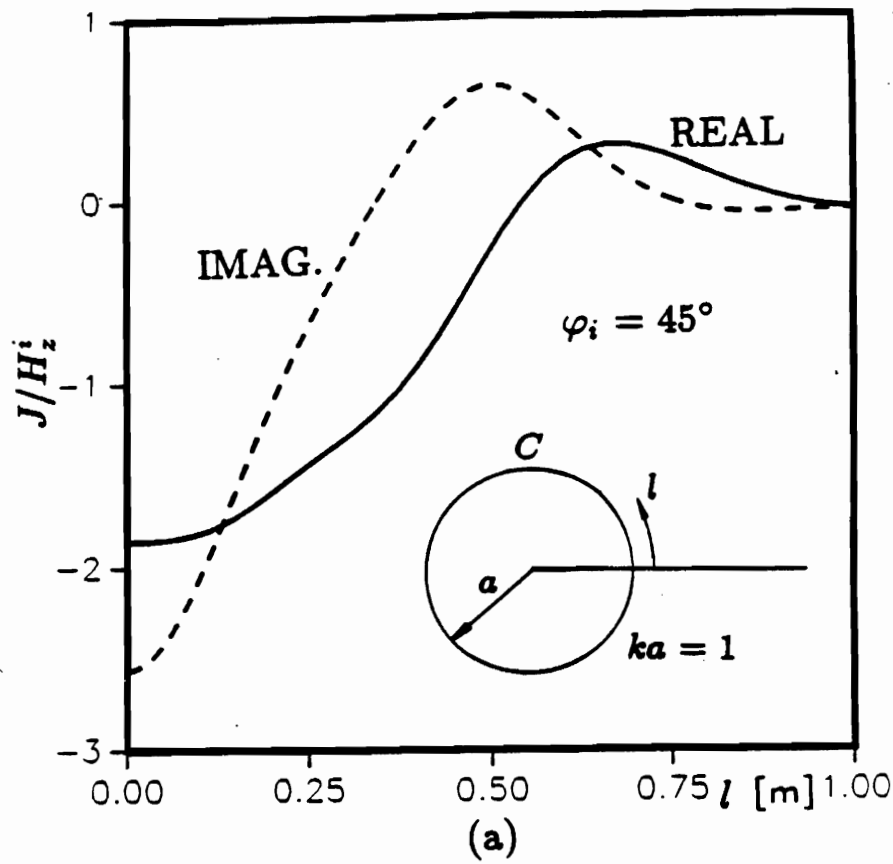


Figure 5.5: (a) Normalized current density on C and (b) far field pattern for a cylindrically tipped half-plane ($\alpha = 0^\circ$) illuminated by a plane wave with $\varphi_i = 45^\circ$.

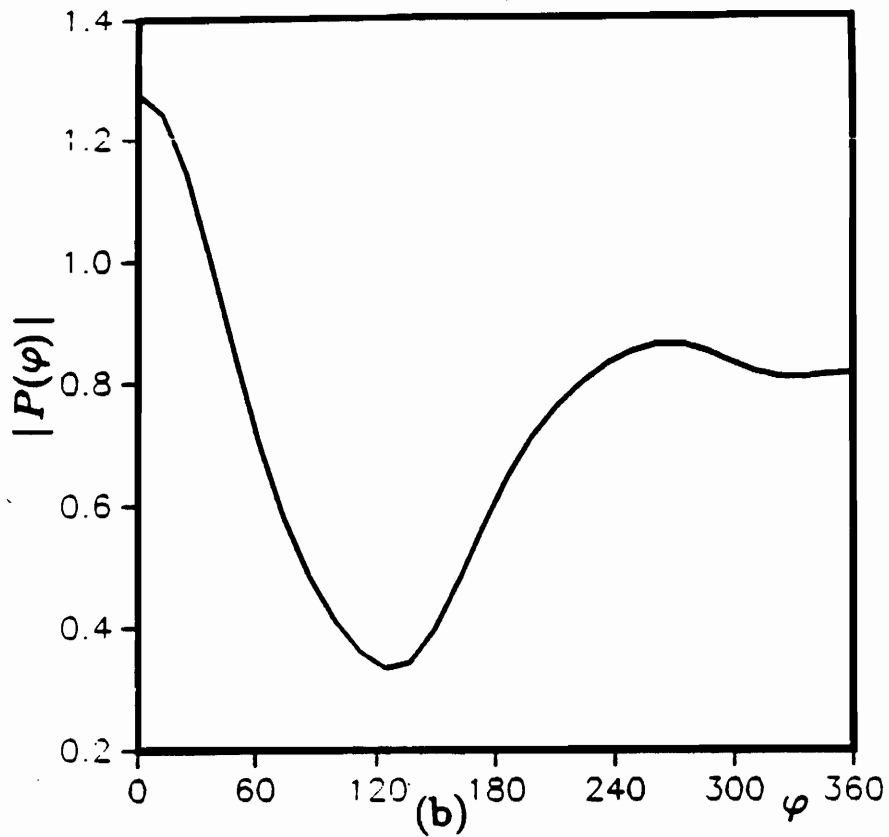
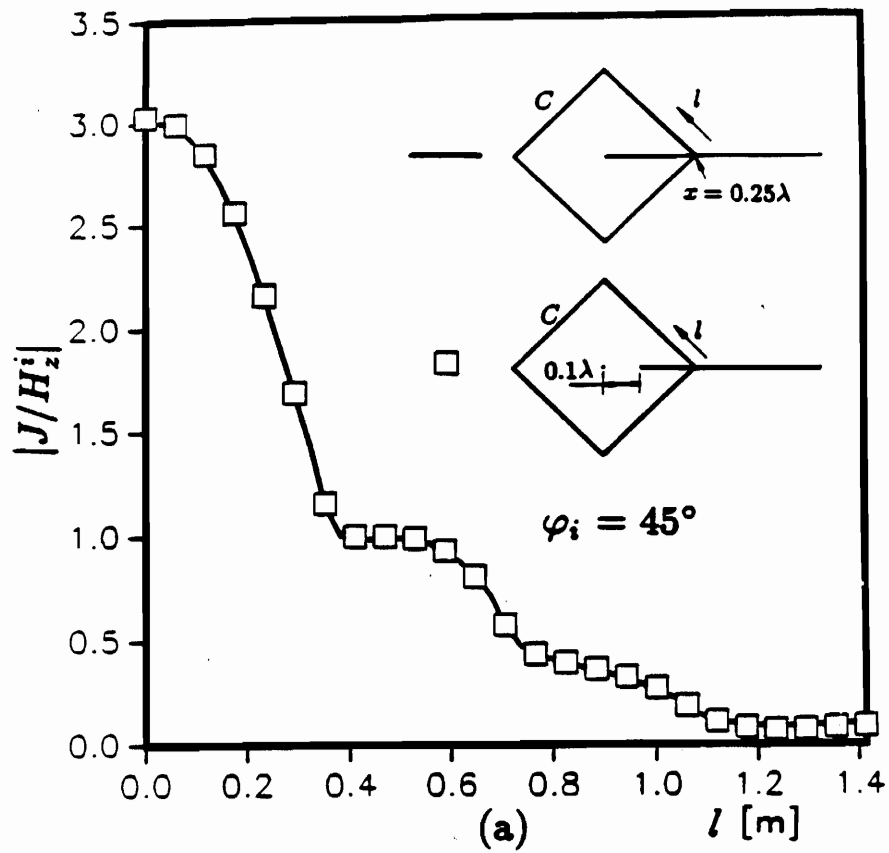


Figure 5.6: (a) Magnitude of the normalized current density on C and (b) far field pattern for a half-plane ($\alpha = 0^\circ$) with the edge enclosed by a square box and illuminated by a plane wave with $\varphi_i = 45^\circ$.

Chapter 6

Electromagnetic Field and Conduction Current Equivalence In the Lorentz and Coulomb Gauges

Coulomb and Lorentz gauge equivalence of the electric and magnetic fields and the conduction current in the time and spectral domains is demonstrated in terms of potentials that are derived subject to the Coulomb and Lorentz gauges. The analysis relies entirely on the Green's functions for both scalar and vector potentials in the two gauges. It is shown that the non-causal portion of the Coulomb gauge electric field expression is removed by the Coulomb gauge vector potential Green's function. The fact that the current is gauge invariant has important implications in the verification of electromagnetic field numerical codes based on integral equation methods.

6.1 Introduction

It is well known that the electromagnetic field can be expressed in terms of potentials whose defining equations are determined, subject to Maxwell's equations, by the choice of gauge and by the currents and charges that ultimately initiate the field. Because the fields are unique, that is, independent of the many possible choices of gauge, they are said to be gauge invariant [25]. Probably, the two most common gauges associated with the electromagnetic fields are the Lorentz and Coulomb gauges. Usually in classical field analysis, the Lorentz gauge is preferred, but in quantum field theory it is often the case that the Coulomb gauge produces a set of equations with reduced degrees of freedom [26].

The Coulomb gauge used in classical field analysis has an interesting characteristic in that the scalar potential is non-causal. This means that when a source is turned on, its scalar potential is seen immediately throughout space and is therefore independent of the speed of light. It was suggested in a paper by Brill and Goodman [16] that this non-causal behavior is

canceled by the transversal current that appears in the Coulomb gauge vector potential equation. Their contention was supported by a mathematical analysis, carried out in the frequency domain and relying on the transversality of the current, proving that the fields expressed in terms the scalar and vector potentials and derived by imposing the Lorentz and Coulomb gauges are equal.

It is the purpose of this chapter to show, relying entirely on the Green's functions in the two gauges, that the Lorentz and Coulomb gauges produce the same electromagnetic fields. The vector potential Coulomb gauge Green's function has, to our knowledge, only recently been derived [27,28]. By taking an approach which depends only on the respective Green's functions we are able to demonstrate that the current as well as the field is gauge invariant. The fact that the current is gauge invariant is important to numerical analysts who perform integral equation formulations based on different gauges. Also we will arrive at a somewhat different view of the mechanism by which the non-causality in the Coulomb gauge field is removed than was put forward in Brill and Goodman's paper.

6.2 Analysis

6.2.1 Time Domain

Our goal is to show equivalence between the electric and magnetic fields expressed in terms of the vector (\mathbf{A}) and scalar (ϕ) potentials which are calculated in the Lorentz and Coulomb gauges. First in the time domain fields

$$\mathbf{E} = -\frac{\partial}{\partial t}\mathbf{A} - \nabla\phi \quad (6.1)$$

$$\mathbf{H} = \frac{1}{\mu}\nabla \times \mathbf{A} \quad (6.2)$$

are expressed in terms of potentials

$$\phi = \frac{1}{\epsilon} \iint_{-\infty}^{\infty} G_{\phi}(R, T) \rho(\mathbf{r}', t') d^3r' dt' \quad (6.3)$$

$$\mathbf{A} = \mu \iint_{-\infty}^{\infty} \bar{\mathbf{G}}_A(R, T) \cdot \mathbf{J}(\mathbf{r}', t') d^3r' dt' \quad (6.4)$$

$$R = |\mathbf{r} - \mathbf{r}'|, T = t - t'$$

In (6.3) and (6.4) the time convention is $\exp(j\omega t)$, respectively G_ϕ, \bar{G}_A are the scalar and dyadic vector potential Green's functions, ρ, \mathbf{J} are electric charge and current and μ, ϵ are the free space permeability and permittivity.

In the time domain our task can best be accomplished, not by dealing directly with the Green's functions in each gauge but rather by showing that the expressions for the difference (\mathbf{E}^d and \mathbf{H}^d) between the fields in the two gauges are identically zero. We begin by subtracting the Lorentz gauge electric field (\mathbf{E}^L) expression from that of the Coulomb gauge (\mathbf{E}^C). The result is

$$\begin{aligned} \mathbf{E}^d &= \mathbf{E}^C - \mathbf{E}^L \\ &= -\mu \frac{\partial}{\partial t} \iint_{-\infty}^{\infty} \bar{\mathbf{G}}_A^d(R, T) \cdot \mathbf{J}(\mathbf{r}', t') d^3 r' dt' - \frac{1}{\epsilon} \nabla \iint_{-\infty}^{\infty} G_\phi^d(R, T) \rho(\mathbf{r}', t') d^3 r' dt' \end{aligned} \quad (6.5)$$

It has been shown previously [27] that in the frequency domain the free space scalar and vector potential difference Green's functions, respectively $\bar{\mathbf{G}}_A^d$ and G_ϕ^d , are

$$\bar{\mathbf{G}}_A^d(\omega) = \frac{1}{k^2} \nabla \nabla \left(\frac{e^{-jkR} - 1}{R} \right) \quad (6.6)$$

$$G_\phi^d(\omega) = -\frac{e^{-jkR} - 1}{R} \quad (6.7)$$

where $k = \omega(\mu\epsilon)^{\frac{1}{2}}$. In terms of the distance parameter R , (6.6) and (6.7) can be expanded into the infinite series

$$\bar{\mathbf{G}}_A^d(\omega) = -\frac{1}{4\pi} \sum_{n=1}^{\infty} \frac{(-jk)^{n-1}}{(n+1)!} \nabla \nabla R^n \quad (6.8)$$

$$G_\phi^d(\omega) = -\frac{1}{4\pi} \sum_{n=1}^{\infty} \frac{(-jk)^{n+1}}{(n+1)!} R^n \quad (6.9)$$

When the time domain form of (6.8), which can be easily found by Fourier transformation according to the definition

$$U(T) = \frac{1}{2\pi} \int_{-\infty}^{\infty} U(\omega) e^{-j\omega T} d\omega, \quad (6.10)$$

is substituted into the first term on the right hand side (RHS) of (6.5), the result is

$$I = \frac{\eta}{4\pi} \sum_{n=1}^{\infty} \frac{1}{(n+1)!} \frac{1}{c^n} \frac{\partial^n}{\partial t^n} \nabla \int_{-\infty}^{\infty} R^n \nabla' \cdot \mathbf{J}(\mathbf{r}', t) d^3 r' \quad (6.11)$$

In obtaining (6.11) we have used the identities

$$\frac{1}{2\pi} \iint_{-\infty}^{\infty} (-jk)^n F_1(\omega) F_2(t') e^{-j\omega T} d\omega dt' = \frac{1}{c^n} \frac{\partial^n}{\partial t^n} \int_{-\infty}^{\infty} F_1(T) F_2(t') dt' \quad (6.12)$$

$$\int_{-\infty}^{\infty} \nabla \nabla R^n \cdot \mathbf{J}(\mathbf{r}', t) d^3 r' = \nabla \int_{-\infty}^{\infty} R^n \nabla' \cdot \mathbf{J}(\mathbf{r}', t) d^3 r' \quad (6.13)$$

and the definition $\eta = (\mu/\epsilon)^{\frac{1}{2}}$ in free space.

Next we turn our attention to the scalar potential portion of Eqn. (6.5). The scalar time domain difference Green's function can once again be found by Fourier transformation of, in this case, Eqn. (6.9). The result when substituted into the second term on the RHS of (6.5), and by again applying (6.12), is

$$II = \frac{\eta}{4\pi} \sum_{n=1}^{\infty} \frac{1}{(n-1)!} \int_{-\infty}^{\infty} \left(\frac{R}{c}\right)^n \frac{\partial^{n+1}}{\partial t^{n+1}} \rho(\mathbf{r}', t) d^3 r' \quad (6.14)$$

The continuity condition

$$\frac{\partial}{\partial t} \rho = -\nabla \cdot \mathbf{J} \quad (6.15)$$

is used to reduce (6.14) to

$$II = -\frac{\eta}{4\pi} \sum_{n=1}^{\infty} \frac{1}{(n+1)!} \frac{1}{c^n} \frac{\partial^n}{\partial t^n} \nabla \int_{-\infty}^{\infty} R^n \nabla' \cdot \mathbf{J}(\mathbf{r}', t) d^3 r' \quad (6.16)$$

Eqns. (6.11) and (6.16) when added together to form the R.H.S. of (6.5) give the expected result $\mathbf{E}^C - \mathbf{E}^L = 0$.

The procedure described above is repeated for the magnetic field. The magnetic difference field with the time domain series form of (6.8) of the magnetic vector potential (6.4) becomes

$$\mathbf{H}^C - \mathbf{H}^L = \frac{1}{4\pi} \nabla \times \sum_{n=1}^{\infty} \frac{(-1)^n}{(n+1)!} \frac{\partial^{n-1}}{\partial t^{n-1}} \int_{-\infty}^{\infty} \nabla \nabla R^n \cdot \mathbf{J}(\mathbf{r}', t) d^3 r' \quad (6.17)$$

Here it is only necessary to show that

$$\nabla \times (\nabla \nabla R^n \cdot \mathbf{J}(\mathbf{r}', t)) = 0 \quad (6.18)$$

In doing this we first note that

$$\nabla \nabla R^n \cdot \mathbf{J}(\mathbf{r}', t) = n R^{n-2} [\mathbf{J} + (n-2) \hat{\mathbf{R}} \hat{\mathbf{R}} \cdot \mathbf{J}] \quad (6.19)$$

where $\hat{\mathbf{R}}$ is the unit vector of \mathbf{R} . With some simple algebraic manipulations one can easily prove that

$$\nabla \times (R^{n-2} \mathbf{J}) = -(n-2) R^{n-3} \mathbf{J} \times \hat{\mathbf{R}} \quad (6.20)$$

$$\nabla \times (R^{n-2} \hat{\mathbf{R}} \hat{\mathbf{R}} \cdot \mathbf{J}) = R^{n-3} \mathbf{J} \times \hat{\mathbf{R}} \quad (6.21)$$

These two equations when substituted into (6.19) lead to the conclusion that $\mathbf{H}^C - \mathbf{H}^L = 0$.

Having shown that the difference in the electric and magnetic fields in the two gauges is zero we can conclude that the two gauges produce the same fields. Because this proof relies only on the Green's functions and not upon the current density \mathbf{J} then the current can also be said to be gauge invariant.

The method, presented above though mathematically correct, may not satisfy the 'purest' who would prefer to simply deal with the full time domain Green's functions in each gauge and show equivalence between the resulting fields. Although this is formally possible, the mathematical procedures for such an approach are much more tedious than the one presented above.

Some reflections on Eqns. (6.3) and (6.4) suggest that there is an easier way to prove equivalence of the electromagnetic field expressed in terms of different gauges. First of all, it is clear that the time integration in (6.3) and (6.4) can be removed and the frequency domain equations recovered by inverse Fourier transformation of (6.1) and (6.2). The simplification of these equations produced by removing one integration (time) greatly reduces the complexity of the resulting proof of equivalence. It is this observation that Brill and Goodman [3] took

advantage of, although they did not work directly with Coulomb gauge Green's functions, when they presented their proof of equivalence in the frequency domain. By continuing to follow this line of thought we are led to the conclusion that if the remainder of the integrations in (3) and (4) are removed then we should arrive at a set of equations for which the proof of equivalence is reduced to a set of algebraic manipulations. This is the approach we take below whereby equivalence is shown in the spectral domain.

6.2.2. Spectral Domain

The spectral domain potentials in the Lorentz gauge can be found by taking the Fourier transform,

$$\tilde{U}(\mathbf{K}) = \frac{1}{(2\pi)^3} \int_{-\infty}^{\infty} U(\mathbf{r}) e^{-j\mathbf{K}\cdot\mathbf{r}} d^3r \quad (6.22)$$

$$\mathbf{K} = k_x \hat{\mathbf{x}} + k_y \hat{\mathbf{y}} + k_z \hat{\mathbf{z}}, \quad (6.23)$$

of the defining equations for the frequency domain scalar and vector potentials, which are respectively

$$\nabla^2 \phi + k^2 \phi = \frac{1}{j\omega\epsilon} \nabla \cdot \mathbf{J} \quad (6.24)$$

$$\nabla^2 \mathbf{A} + k^2 \mathbf{A} = -\mu \mathbf{J} \quad (6.25)$$

By carrying out this procedure it is a simple matter to show that

$$\tilde{\phi} = -\frac{\mathbf{K}}{\omega\epsilon(K^2 - k^2)} \cdot \tilde{\mathbf{J}} \equiv \tilde{\mathbf{G}}_{\phi} \cdot \tilde{\mathbf{J}} \quad (6.26)$$

$$\tilde{\mathbf{A}} = \frac{\mu \bar{\mathbf{I}}}{K^2 - k^2} \cdot \tilde{\mathbf{J}} \equiv \tilde{\mathbf{G}}_{\mathbf{A}} \cdot \tilde{\mathbf{J}} \quad (6.27)$$

where $K = |\mathbf{K}|$ and $\bar{\mathbf{I}} = \hat{\mathbf{x}}\hat{\mathbf{x}} + \hat{\mathbf{y}}\hat{\mathbf{y}} + \hat{\mathbf{z}}\hat{\mathbf{z}}$ is the identity dyadic. The tilde (\sim) indicates that the associated letter symbol is now a spectral domain quantity.

The frequency domain electric and magnetic fields

$$\mathbf{E} = -j\omega \mathbf{A} - \nabla \phi \quad (6.28)$$

$$\mathbf{H} = \frac{1}{\mu} \nabla \times \mathbf{A} \quad (6.29)$$

transformed into the spectral domain become

$$\tilde{\mathbf{E}} = -j\omega\tilde{\mathbf{A}} - j\mathbf{K}\tilde{\phi} \quad (6.30)$$

$$\tilde{\mathbf{H}} = \frac{1}{\mu}\mathbf{K} \times \tilde{\mathbf{A}} \quad (6.31)$$

All relevant equations have now been reduced to simple vector algebraic form. Direct substitution of (6.26) and (6.27) into (6.30) and (6.31) gives

$$\tilde{\mathbf{E}} = \frac{j\omega\mu}{k^2} \left(\frac{\mathbf{K}\mathbf{K} - \bar{\mathbf{I}}k^2}{K^2 - k^2} \right) \cdot \tilde{\mathbf{J}} \quad (6.32)$$

$$\tilde{\mathbf{H}} = -\frac{\mathbf{K} \times \tilde{\mathbf{J}}}{K^2 - k^2} \quad (6.33)$$

In the Coulomb gauge the frequency domain scalar and vector potential defining equations are [25]

$$\nabla^2\phi^C = \frac{1}{j\omega\epsilon}\nabla \cdot \mathbf{J} \quad (6.34)$$

$$\nabla^2\mathbf{A}^C + k^2\mathbf{A}^C = -\mu\mathbf{J} + j\omega\mu\epsilon\nabla\phi^C \quad (6.35)$$

Fourier transformation of (6.34) according to (6.22) produces the spectral domain equation

$$\tilde{\phi}^C = -\frac{\mathbf{K}}{\omega\epsilon K^2} \cdot \tilde{\mathbf{J}} \equiv \tilde{\mathbf{G}}_\phi^C \cdot \tilde{\mathbf{J}} \quad (6.36)$$

This result when substituted into the spectral domain form of (35)

$$\tilde{\mathbf{A}}^C = \mu \left(\frac{\tilde{\mathbf{J}} + \omega\epsilon\mathbf{K}\tilde{\phi}^C}{K^2 - k^2} \right) \quad (6.37)$$

gives

$$\tilde{\mathbf{A}}^C = \frac{\mu}{K^2} \left(\frac{\bar{\mathbf{I}}K^2 - \mathbf{K}\mathbf{K}}{K^2 - k^2} \right) \cdot \tilde{\mathbf{J}} \equiv \tilde{\mathbf{G}}_A^C \cdot \tilde{\mathbf{J}} \quad (6.38)$$

Equations (6.36) and (6.38) when substituted into (6.30) and (6.31) readily reduce to (6.32) and (6.33) which were obtained above with the Lorentz gauge.

Perhaps the clearest indication as to how the non-causal Coulomb gauge term is removed is provided by the spectral domain equations in the paragraphs above. Because of the pole

singularities at $K = \pm k$, inverse Fourier transformation of (6.26), (6.27) and (6.38) will always yield causal results. On the other hand, in (6.36) and (6.38), as well as (6.26) and (6.27), result in the fields (6.32) and (6.33), neither of which contain a pole at the origin. Therefore, the non-causal nature of the Coulomb gauge scalar potential is independent of the exciting current, only an artifact of the gauge, and is mathematically removed by the vector potential Green's function which cancels the scalar potential pole singularity at the origin.

6.3 Discussion and Conclusion

Equivalence and therefore gauge invariance of the electromagnetic field expressed in terms of Lorentz and Coulomb gauge potentials has been shown. Two proofs of field equality have been presented, one in the time domain which relies on the difference between the Coulomb and Lorentz gauge Green's functions and another significantly simpler proof in the spectrum domain. The proofs provided here are different from the frequency domain method presented in the classic paper by Brill and Goodman [16] because here only the properties of the Green's functions in the two gauges are used to show equivalence. More importantly the transversality property of the conduction current is not required in our analysis. Since this is the case we are led below to a somewhat different view of the non-causal nature of the Coulomb scalar potential field than that offered in [16].

An erroneous conclusion that one could draw by attempting to assign a physical interpretation to the R.H.S. of (6.35) is that since the Coulomb vector potential can arise strictly from the transverse current, which is defined to be

$$\mathbf{J}_{\perp} = \mathbf{J} - j\omega\epsilon\nabla\phi,$$

then the current itself can in some way effect causality. Brill and Goodman state “ \mathbf{J}_{\perp} compensates for the apparent instantaneous Coulomb interaction appearing in the expression for \mathbf{E}^C ”. This remark can be accepted only if the current \mathbf{J} is viewed as a purely mathematical quantity baring no resemblance to physical reality. This is because the transverse current is not a physically separate part of the actual impressed or conduction current on a body but rather a totally nonphysical entity whose mathematical representation exists throughout coordinate (Euclidian) space [10]. On the other hand, the Green's function is a non-physical, non-unique quantity, whose mathematical form depends upon the chosen gauge. Therefore, based on the analysis presented above, where a purely physical current is retained throughout, it is clear that

in the Coulomb gauge the non-causal nature of the scalar potential is due entirely to the scalar potential Green's function and is canceled by the vector potential Green's function.

Finally, on a different subject, it has been speculated that because in quantum field theory the Coulomb gauge is most often applied in momentum space, whose dual is the spectral domain in classical electromagnetism, a spectral domain integral equation formulation in the Coulomb gauge may have some advantage over that in the Lorentz gauge. However, the spectral domain analysis presented in this paper suggests that this is not the case. In fact, because the electromagnetic field equations in the spectral domain are entirely algebraic, the free space and vector potential portions of the field can be arranged so that the field expressions (6.32) and (6.33) are always the same regardless of gauge.

Chapter 7

Time Domain Scattering Calculations in the Coulomb Gauge

The possibility of implementing the Coulomb gauge in time domain electric field integral equation numerical calculations is examined. Two formulations are explored including the use of a solenoid current and replacement of the Lorentz gauge Green's function with that of the Coulomb gauge. It is shown that the Coulomb gauge involves a 3-D integration and solution of a matrix equation at each time step while the Lorentz gauge requires a 2-D integration and no matrix equation.

7.1 Introduction

The Lorentz gauge is the preferred gauge when problems in electromagnetic scattering and diffraction are solved by the classical approach involving a scalar potential ϕ and a vector potential \mathbf{A} . In this gauge

$$\nabla \cdot \mathbf{A} + \frac{1}{c^2} \frac{\partial \phi}{\partial t} = 0.$$

For a perfectly conducting scatterer, the Electric Field Integral Equation (EFIE)

$$\left[\frac{\partial \mathbf{A}}{\partial t} + \nabla \phi \right]_{\text{tan}} = \mathbf{E}_{\text{tan}}^{\text{inc}}$$

then determines the surface currents \mathbf{J} and surface charges ρ .

This formalism can be exploited to obtain an explicit time marching scheme in which the currents \mathbf{J}^k and charges ρ^k at time step $k\Delta t$ are calculated from the currents and charges calculated at earlier time steps (and the exciting field). This scheme is *stable* only when $c\Delta t$ is chosen smaller than the minimum spatial separation of current sample points on the surface of the scatterer. In addition, for closed bodies, an averaging procedure must be used to suppress the growth of non-physical oscillations corresponding to interior resonant cavity modes occurring at frequencies at which the frequency domain EFIE has non-unique solutions.

The question arises: are these features of stability and instability artifacts of the gauge condition, and can they be avoided by choice of another gauge? We examine particularly the Coulomb gauge.

7.2 Formulation

Let us begin by reviewing the usual Lorentz gauge formulation and then examine the other gauge. In either gauge the electric field \mathbf{E} and the magnetic flux density \mathbf{B} are expressed in terms of a vector potential \mathbf{A} and a scalar potential ϕ via

$$\mathbf{B} = \nabla \times \mathbf{A}, \quad \mathbf{E} = -\frac{\partial \mathbf{A}}{\partial t} - \nabla \phi,$$

It follows that

$$\left(\nabla^2 \mathbf{A} - \frac{1}{c^2} \frac{\partial^2 \mathbf{A}}{\partial t^2}\right) - \nabla \left(\nabla \cdot \mathbf{A} + \frac{1}{c^2} \frac{\partial \phi}{\partial t}\right) = -\mu \mathbf{J},$$

where \mathbf{J} represents the surface current on the scatter S . The charge density ρ on the surface is obtained from

$$\frac{\partial \rho}{\partial t} + \nabla_o \cdot \mathbf{J} = 0,$$

where $\nabla_o \cdot \mathbf{J}$ denotes the surface divergence of \mathbf{J} .

If we use \mathbf{A}^L, ϕ^L to denote the potentials in the Lorentz gauge, then the gauge condition reads

$$\nabla \cdot \mathbf{A}^L + \frac{1}{c^2} \frac{\partial \phi^L}{\partial t} = 0.$$

Consequently,

$$\begin{aligned} \nabla^2 \mathbf{A}^L - \frac{1}{c^2} \frac{\partial^2 \mathbf{A}^L}{\partial t^2} &= -\mu \mathbf{J}, \\ \nabla^2 \phi^L - \frac{1}{c^2} \frac{\partial^2 \phi^L}{\partial t^2} &= -\rho/\epsilon, \end{aligned}$$

so that

$$\begin{aligned} \mathbf{A}^L(\mathbf{r}, t) &= \frac{\mu}{4\pi} \int_S \frac{\mathbf{J}(\mathbf{r}', \tau)}{R} dS', \\ \phi^L(\mathbf{r}, t) &= \frac{1}{4\pi\epsilon} \int_S \frac{\rho(\mathbf{r}', \tau)}{R} dS', \end{aligned}$$

where $\mathbf{R} = |\mathbf{r} - \mathbf{r}'|$, $\tau = t - R/c$ represents "retarded time," and $c = 1/(\mu\epsilon)^{1/2}$ is the speed of light.

To obtain a numerical scheme based on this formulation we collect the relevant equations

$$\frac{\partial \rho}{\partial t} + \nabla_o \cdot \mathbf{J} = 0 \tag{7.1}$$

$$\phi^L(\mathbf{r}, t) = \frac{1}{4\pi\epsilon} \int_S \frac{\rho(\mathbf{r}', \tau)}{R} dS' \quad (7.2)$$

$$\hat{\mathbf{n}} \times \left[\frac{\partial \mathbf{A}^L}{\partial t} + \nabla \phi^L \right] = \hat{\mathbf{n}} \times \mathbf{E}^s \quad (7.3)$$

$$\mathbf{A}^L(\mathbf{r}, t) = \frac{\mu}{4\pi} \int_S \frac{\mathbf{J}(\mathbf{r}', \tau)}{R} dS'. \quad (7.4)$$

Here $\hat{\mathbf{n}}$ denotes the unit outward normal to the surface S of the scatterer.

Let us use central differences to approximate (7.1) and (7.3). Upon discretization equation (7.1) relates to ρ^{k+1} at time step $(k+1)\Delta t$ to the charge ρ^k at the previous time step and to the current $\mathbf{J}^{k+\frac{1}{2}}$ at an intermediate time value. Equation (7.2) can then utilize the charge update to calculate the scalar potential ϕ^L at time step $(k+1)\Delta t$. Next $\hat{\mathbf{n}} \times \mathbf{A}^L$ at time step $\left(k + \frac{3}{2}\right)\Delta t$ can be calculated from values of $\hat{\mathbf{n}} \times \mathbf{A}^L$ at $\left(k + \frac{1}{2}\right)\Delta t$ and $\nabla \phi^L$ at $(k+1)\Delta t$. Finally, equation (7.4) can be used to determine the surface current $\mathbf{J}^{k+\frac{3}{2}}$ by using the vector potential values at this time step, and splitting the surface integral in (7.4) into a self-patch term, involving the contribution from $\mathbf{J}^{k+\frac{3}{2}}$ and a non-self-patch term, involving contributions from the surface current at *earlier* time steps (which have therefore already been computed). The details of this method, its accuracy, its stability properties and techniques for stabilizing the evolving numerical solution are discussed in detail in [30].

Turning to the Coulomb gauge – in which the vector and scalar potential will be denoted \mathbf{A}^C, ϕ^C – we can develop an analogous formalism. In this gauge $\nabla \cdot \mathbf{A} = 0$ so that

$$\nabla^2 \mathbf{A}^C - \frac{1}{c^2} \frac{\partial^2 \mathbf{A}^C}{\partial t^2} = -\mu \mathbf{J}^s,$$

where \mathbf{J}^s denotes the *solenoidal* current

$$\mathbf{J}^s = \mathbf{J} - \epsilon \frac{\partial}{\partial t} (\nabla \phi^C),$$

and

$$\nabla^2 \phi^C = -\rho/\epsilon.$$

Thus, the *scalar* potential

$$\phi^C(\mathbf{r}, t) = \frac{1}{4\pi\epsilon} \int_S \frac{\rho(\mathbf{r}', t)}{R} dS'$$

involves **no** retarded quantities, whereas the vector potential

$$\mathbf{A}^C(\mathbf{r}, t) = \frac{\mu}{4\pi} \int_{\mathbf{R}^3} \frac{\mathbf{J}^s(\mathbf{r}', \tau)}{R} dV'.$$

involves an integral over all space of the *retarded* solenoidal current. Notice that the region of integration is **finite** since \mathbf{J}^s is zero at any time before the incident field strikes the body. However, notice that \mathbf{J}^s is generally nonzero outside the scatterer - in contrast to the (physical) surface current \mathbf{J} which is nonzero *only* on the scatterer.

Let us assemble the equations for marching-in-time in the Coulomb gauge:

$$\frac{\partial \rho}{\partial t} + \nabla_{\mathbf{o}} \cdot \mathbf{J} = 0 \quad (7.5)$$

$$\phi^C(\mathbf{r}, t) = \frac{1}{4\pi\epsilon} \int_S \frac{\rho(\mathbf{r}', t)}{R} dS' \quad (7.6)$$

$$\hat{\mathbf{n}} \times \left[\frac{\partial \mathbf{A}^C}{\partial t} + \nabla \phi^C \right] = \hat{\mathbf{n}} \times \mathbf{E}^i \quad (7.7)$$

$$\hat{\mathbf{n}} \times \mathbf{A}^C(\mathbf{r}, t) = \hat{\mathbf{n}} \times \frac{\mu}{4\pi} \int_{\mathbf{R}^3} \frac{\mathbf{J}^s(\mathbf{r}', \tau)}{R} dV' \quad (7.8)$$

$$\hat{\mathbf{n}} \times \mathbf{J} = \hat{\mathbf{n}} \times \mathbf{J}^s + \hat{\mathbf{n}} \times \epsilon \frac{\partial}{\partial t} (\nabla \phi^C) \quad (7.9a)$$

$$\hat{\mathbf{n}} \cdot \mathbf{J} = \hat{\mathbf{n}} \cdot \mathbf{J}^s + \hat{\mathbf{n}} \cdot \epsilon \frac{\partial}{\partial t} (\nabla \phi^C). \quad (7.9b)$$

As before (7.5) allows charge updates, and (7.6) permits update of the scalar potential ϕ^C at time step $(k+1)\Delta t$. Likewise (7.7) allows an update of the potential \mathbf{A}^C in terms of previously calculated quantities. From (7.8) we can extract the solenoidal current \mathbf{J}^s by a splitting of the integral into contributions relating to $(\mathbf{J}^s)^{k+\frac{3}{2}}$ and earlier time contributions. Finally, (7.9a) and (7.9b) enable the calculation of the surface physical current \mathbf{J} -provided an estimate for $\frac{\partial}{\partial t}(\nabla \phi^C)$ is based, not on central differences, but on the approximating formula

$$\frac{2f^{k+1} - 3f^k + f^{k-1}}{\Delta t} = (f')^{k+\frac{3}{2}} + O((\Delta t)^2).$$

While formally similar to the Lorentz gauge calculation, the above Coulomb gauge calculation encounters several serious difficulties. These difficulties are essential due to the fact that the solenoidal current \mathbf{J}^s is nonzero throughout all space rather than confined

While formally similar to the Lorenz gauge calculation, the above Coulomb gauge calculation encounters several serious difficulties. These difficulties are essential due to the fact that the solenoidal current \mathbf{J}^s is nonzero throughout all space rather than confined to the surface. Thus, the integration in (7.8) is a *volume* integral, rather than a surface integral and, as time progresses, the volume of integration *expands*. In addition, the time marching procedure relies on the EFIE (7.7), which is an equation on the surface, so we can only obtain surface quantities from this. To obtain the values of \mathbf{J}^s off the surface required to evaluate (7.8) it is necessary to use the equation

$$\mathbf{J}^s = -\varepsilon \frac{\partial}{\partial t} (\nabla \phi^C)$$

together with the integral (7.6) to evaluate ϕ^C . Thus, to evaluate the 3-D integral (7.8), we have to perform a 2-D integration to obtain the value of the integrand in (7.8) at each point. This equivalent to performing a 5-D integration, which is clearly extremely costly and unwieldy in comparison with the 2-D integration required in the Lorenz calculation. As a general observation in scattering problems, integral equation methods are designed to avoid calculation on 3-D grids by performing calculations only on 2-D surfaces: in fact if one is willing to use 3-D grids, then other approaches, e.g. finite difference time-domain (FDTD), are much more effective. Also, the complexity of the calculation makes one doubt whether reliable results could be obtained from it.

There is an alternative to equation (7.8) which avoids some of these problems by using a solenoidal Green's function $\bar{\mathbf{G}}^C$ ($\bar{\mathbf{G}}^C$ is a dyadic function). This leads to an equation of the form

$$\mathbf{A}^C(\mathbf{r}, t) = \mu \int_S \int_{-\infty}^t \bar{\mathbf{G}}^C(\mathbf{r}, \mathbf{r}', t, t') \cdot \mathbf{J}(\mathbf{r}', t') dt' dS' \quad (7.10)$$

The dyadic function $\bar{\mathbf{G}}^C$, which is found by Fourier transformation of the frequency domain Coulomb gauge Green's function in [3], is

$$\bar{\mathbf{G}}^C = \frac{\bar{\mathbf{I}}}{4\pi R} \left[\left(\frac{c}{R}\right)^2 v(\tau - t') + \left(\frac{c}{R}\right) u(\tau - t') + \delta(\tau - t') - \left(\frac{c}{R}\right)^2 v(t - t') \right] \quad (7.11)$$

Where \mathbf{R} is the vector defined by $\mathbf{R} = \mathbf{r} - \mathbf{r}'$, $\bar{\mathbf{I}} = \hat{x}\hat{x} + \hat{y}\hat{y} + \hat{z}\hat{z}$ is the idemfactor, $u(x)$ is the unit step function

$$u(x) = \begin{cases} 1; & x > 0 \\ 0; & x < 0, \end{cases}$$

$v(x)$ is the ramp function

$$v(x) = \begin{cases} x; & x > 0 \\ 0; & x < 0, \end{cases}$$

and $\delta(x)$ is the Dirac-delta function.

Equation (7.10) involves the values of the (physical) current \mathbf{J} only on the surface S and so avoids the difficulties involved in using the values of the (non-physical) \mathbf{J}^s off the surface. However, this equation also suffers from certain problems. The form of $\bar{\mathbf{G}}^C$ is such that the integration in (7.10) involves an integration with respect to t' at each \mathbf{r}' . (In the Lorenz gauge the Green's function depends upon time simply via a delta function of the form $\delta(\tau-t')$ so the time integration is trivial). Thus, we are back to a 3-D integration, but involving quantities already calculated, which solves one previous difficulty. However, another difficulty is that (7.10) utilizes the values of $\mathbf{J}(\mathbf{r}',t)$, at all \mathbf{r}' , to evaluate $\mathbf{A}^C(\mathbf{r},t)$, at all \mathbf{r} . Thus, when we discretize the system we end up having to solve a *matrix* equation to extract the values of $\mathbf{J}(\mathbf{r},t), \mathbf{r} \in S$, whereas in the Lorenz case these values were given explicitly.

7.3 Conclusion

To sum up, there are two approaches to numerically computing electromagnetic scattering problems in the Coulomb gauge. The first utilizes the solenoidal current \mathbf{J}^s whereas the second uses the solenoidal Green's function. The first has the computational complexity of a 5-D integration at each step, while the latter involves a 3-D integration, and solution of a matrix equation at each time step. On the other hand use of the Lorenz gauge only requires a 2-D integration and no matrix equation at each time step. In view of the obstacles, it does not seem worth attempting to use the Coulomb gauge numerically (especially as the solenoidal Green's function is much more complicated to evaluate than the usual Green's function). Furthermore, it seems clear from the above discussion that the Lorenz gauge is essentially the only gauge in which the current term which appears in the definition of the vector potential, is genuinely a 2-D quantity restricted to the surface of the scatterer, and so is uniquely suited to time domain calculations. This is in contrast to the steady state of harmonic case where the solenoidal Green's function introduces relatively little extra complexity [31] (though there may be some reduction in convergence rate of any series expressions for the Green's function).

Chapter 8

Conclusions

In this report the Coulomb gauge formulation and solution of the electromagnetic field vector and scalar potential Green's functions are presented for both waveguiding and scattering structures. For the scattering cases presented here the Green's functions are placed in mixed potential electric field integral equations (MPIE's) which are solved by the moment method. Green's functions are derived for free space, the rectangular waveguide and the two-dimensional perfectly conducting cylinder and wedge. Comparisons between the Coulomb and Lorentz gauge formulations are made in terms of analytical difficulty and computer computation time necessary to solve for the current on scatterers of various shapes.

The attractive feature of the Coulomb gauge is that for the cases considered here the Coulomb scalar potential is either mathematically simpler or in closed form, rather than in series form as in the Lorentz gauge. However, this advantage of the Coulomb gauge is to some extent offset by the fact that the resulting vector potential series converge more slowly than the corresponding series of the Lorentz gauge. Therefore acceleration of these series requires more analytical work than is necessary with the corresponding Lorentz gauge. Also, even in cases where the Lorentz vector potential Green's dyadic is diagonal, its Coulomb gauge counterpart is likely to be fully populated. This is true, for instance, for both free space and the rectangular waveguide. However, for the cylinder and the wedge both gauges have fully populated vector potential Green's functions. Consequently, for these two cases, the Coulomb gauge, MPIE's are noticeably more efficient than their Lorentz gauge counterpart, since they do not require summation of scalar potential series. For example, for both the cylinder and the wedge, when 45 basis functions are used to represent the current, a 15%

savings in matrix fill time was realized when the Coulomb gauge was used instead of the Lorentz gauge.

However, this research has shown that the Coulomb gauge is not generally preferable to the Lorentz gauge when the MPIE formulation is used to solve scattering problems in complex environments which admit closed form solutions of the Poisson equation. The number of such geometries in which the Coulomb gauge is an improvement is limited. In addition to the cases presented here the only other three-dimensional problem known to the authors which likely falls into this category is that of the scatterer or antenna of arbitrary shape in the presence of sphere.

It should be pointed out, however, that the Coulomb scalar potential contains the static limit portion of the electromagnetic field. One can therefore isolate and observe the physical behavior of that part of the field (the Coulomb vector potential portion) that approaches zero as the excitation frequency is decreased. This observation may prove useful in electromagnetic compatibility studies.

In conclusion, a major benefit of this research is that we have been able to demonstrate that it is not necessary to solve classical electromagnetic scattering problems with the Lorentz gauge. The Coulomb gauge has been shown to be one alternative, although not generally an improvement.

Bibliography

- [1] Rao, S. M., Wilton, D. R. and Glisson, A. W.: 'Electromagnetic scattering by surfaces of arbitrary shape' *IEEE Trans. Antennas Propag.*, 1982, 30, pp. 409-418.
- [2] Bjorken, J. D., and Drell, S. D. 'Relativistic Quantum Fields,' (McGraw hill, 1965), Sect. 14.2.
- [3] Collin, R. E.: 'Field Theory of Guided Waves,' (McGraw Hill, 1960), Sect. 5.6
- [4] Smythe, W. R.: 'Static And Dynamic Electricity, 3rd ed.,' (Hemisphere, 1989), Chapt. 13, Sect. 13.03.
- [5] E. P. Ekelman and G. A. Thiele, "A hybrid technique for combining the moment method treatment of wire antennas with the GTD for curved surfaces," *IEEE Trans. Antennas Propagat.*, vol. AP-28, pp. 831-838, Nov. 1980.
- [6] Tai, C-T.: 'Dyadic Green's Function Electromagnetic Theory,' (Intext, 1971).
- [7] C-T. Tai, "Eigenfunction Expansion of Dyadic Green's Functions," *Math. Note* 28, Air Force Weapons Lab., Kirtland Air Force Base, N.M., July 1973.
- [8] Van Bladel, J.: 'Electromagnetic Fields,' (Hemisphere, 1985), Chapt. 7.
- [9] Van Bladel, J.: 'Electromagnetic Fields,' (Hemisphere, 1985), A6.22, pg. 542 and no. 28, pg. 508.
- [10] Morris, P. M., and Feshbach, H.: 'Methods of theoretical physics,' (McGraw Hill, 1953), Chapt. 13, Sect. 1.
- [11] R. E. Collin, "On the Incompleteness of E and H Modes in Waveguides," *Can. J. Phys.*, vol. 51, pp. 1135-1140, June 1973.
- [12] P. H. Pathak, "On the Eigenfunction Expansion of Electromagnetic Dyadic Green's Functions," *IEEE Trans. Antennas Propagat.*, vol. AP-31, pp. 837-846, Nov. 1983.
- [13] R. E. Collin, "Dyadic Green's function expansions in spherical coordinates," *Electo-magn.*, vol. 6, no. 3, pp. 183-207, 1986.

- [14] L. W. Pearson, "On the spectral expansion of the electric and magnetic dyadic Green's functions in cylindrical harmonics," *Radio Sci.*, vol. 18, pp. 166-174, Mar.-Apr. 1983.
- [15] R. Plonsey and R. E. Collin, "Principles and Applications of Electromagnetic Fields," (McGraw-Hill, 1961).
- [16] O. L. Brill and B. Goodman, "Causality in the Coulomb gauge," *Am. J. Phys.*, vol. 35, pp. 832-837, 1967.
- [17] J. P. Donohoe, "The dyadic Green's functions of the semi-infinite length tubular cylinder," Ph.D. Dissertation, University of Mississippi, May 1987.
- [18] Abramowitz, M., and I. A. Stegun, eds., "Handbook of Mathematical Functions," (Dover, 1965).
- [19] M. D. G. Karunaratne, K. A. Michalski, and C. M. Butler, "TM scattering from a conducting strip loaded by a dielectric cylinder," *IEE Proc.. Pt. H.*, vol. 132, pp. 115-122, Apr. 1985.
- [20] D. M. Pozar and E. H. Newman, "Near fields of a vector electric line source near the edge of a wedge," *Radio Sci.* vol. 14, pp. 397-403, May-June 1979.
- [21] Glisson, A. W., and D. R. Wilton, "Simple and efficient numerical methods for problems of electromagnetic radiation and scattering from surfaces," *IEEE Trans. Antennas Propagat.*, vol. AP-28, pp. 593-603, Sept. 1980.
- [22] Harrington, R. F., "Time-Harmonic Electromagnetic Fields," (McGraw-Hill, 1961).
- [23] L. B. Felsen and N. Marcuvitz, "Radiation and Scattering of Waves," (Prentice Hall, 1973).
- [24] Karp, S. N., "Diffraction by a tipped wedge with application to blunt edges," *Inst. Of Math. Sci. Rept. EM 52*, New York University, May 1953.
- [25] J. D. Jackson, *Classical Electrodynamics*, 2nd ed., Chapt. 6, John Wiley & Sons, New York, 1975.
- [26] J. D. Bjorken and S. D. Drell, *Relativistic Quantum Fields*, section 14.2, McGraw Hill, New York 1965.

- [27] R. D. Nevels and K. J. Crowell, 'A Coulomb Gauge Analysis of a Wire Scatterer,' IEE Proc. ~ Pt. H, vol. 137, pp. 384-388, Dec. 1990.
- [28] B. P. Rynne, P. D. Smith and R. D. Nevels, 'Time Domain Scattering Calculations in the Coulomb Gauge,' Microwave Opt. Technol. Lett., vol. 4, pp. 586-589, Dec. 1991.
- [29] R. F. Harrington, *Field Computation by the Method of Moments*, McGraw Hill, New York, 1968.
- [30] B. P. Rynne and P. D. Smith, "Stability of Time Marching Algorithms for the Electric Field Integral Equation," *J. Electromagnetic Waves and Applications*. (To appear, 1991).
- [31] K. A. Michalski and R. D. Nevels, "On the Use of the Coulomb Gauge in Solving Source-Excited Boundary Value Problems in Electromagnetics," *IEEE Trans. Microwave Theory Tech*, vol. MTT-36, pp. 1328-1333, Sept. 1988.
- [32] R. D. Nevels and K. J. Crowell, "A Coulomb Gauge Analysis of a Wire Scatterer," *IEE Trans.*, vol. 137, Part H, No. 6, pp. 384-388, Dec. 1990.



TEXAS A&M UNIVERSITY

Department of Electrical Engineering

College Station, Texas 77843-3128

(409) 845-7441

FAX (409) 845-6259

979

February 16, 2001

Dr. Carl E. Baum
AFRL/DEHP Bldg. 909
3550 Aberdeen Ave. SE
Kirtland AFB, NM 87177-556

JN 564

Dear Carl,

Enclosed is the modified version of a short monograph on the Coulomb gauge research we carried out a few years ago. I have added Krys Michalski's name because he was a co contributor to much of the research. The Air Force is granted all the rights and privileges necessary for publication.

Please call if you have questions.

Sincerely,

A handwritten signature in cursive script, appearing to read "Bob".

Robert Nevels
Department of Electrical Engineering
Texas A&M University
College Station, TX 77845-3128

(979) 845-7591
nevels@ee.tamu.edu



